

Genetic engineering of the first functional human cardiomyocyte lines for building clinically relevant atrial fibrillation models

Niels Harlaar^{1,2}, Sven O. Dekker¹, Juan Zhang¹, Marieke W. Veldkamp³, Arie O. Verkerk^{3,4}, Verena Schwach⁵, Carla Cofino Fabres⁵, Lente J.S. Lerink¹, Mathilde R. Rivaud³, Marie José T.H. Goumans⁶, Dobromir Dobrev⁷, Robert J.M. Klautz², Martin J. Schalijs¹, Robert Passier⁵, Thomas J. van Brakel², Daniël A. Pijnappels^{1#}, Antoine A.F. de Vries^{1#*}

¹ Department of Cardiology, Leiden University Medical Center, Leiden, the Netherlands

² Department of Cardiothoracic Surgery, Leiden University Medical Center, Leiden, the Netherlands

³ Department of Clinical and Experimental Cardiology, Amsterdam UMC, Amsterdam, the Netherlands

⁴ Department of Medical Biology, Amsterdam UMC, Amsterdam, the Netherlands

⁵ Applied Stem Cell Technologies, University of Twente, Enschede, the Netherlands

⁶ Department of Cell and Chemical Biology, Leiden University Medical Center, Leiden, the Netherlands

⁷ Institute of Pharmacology, West German Heart and Vascular Center, University Duisburg-Essen, Essen, Germany

#Shared senior authorship

*Email: hiam@lumc.nl

ABSTRACT

The development of clinically relevant *in vitro* models of human disease has created a large demand for human parenchymal cells like cardiomyocytes, hepatocytes and neurons. Although recent progress in pluripotent stem cell technology has greatly advanced the development of human disease models, several challenges remain regarding their scalability, representativeness and reproducibility. For example, the lack of a robust and abundant source of well-differentiated human atrial myocytes (AMs) has been impeding the generation of representative *in vitro* models for human atrial fibrillation (AF), the most prevalent heart rhythm disorder. Here, we show how a lentiviral vector-based conditional cell immortalization procedure allows mass production (through quadrillion-fold multiplication) of fully functional (*i.e.* excitable and contractile) human AMs. Neither cryopreservation, nor the use of different sources of fetal bovine serum or passage history compromised their cardiomyogenic differentiation ability. The robust proliferation and differentiation of these human immortalized AMs (hiAMs) enabled the creation of scalable human models of AF, in which fibrillatory activity not only resembles clinical AF manifestation (*e.g.* activation frequencies of 6-8 Hz), but can also be terminated by antiarrhythmic drugs used in clinical practice. This study exemplifies the utility of our conditional cell immortalization technology to generate monoclonal lines of human parenchymal cells with preserved differentiation capacity for the development of representative human *in vitro* models for disease phenotyping and mechanistic studies along with drug discovery and therapeutic testing.

INTRODUCTION

Preclinical biomedical research across academia and industry strongly relies on *in vitro* models to advance pathophysiological insight and develop novel therapeutics. Human disease models based on (cultured) animal cells are becoming less popular due to 1) the growing awareness of the existence of principal differences in (patho)physiology between humans and animals and 2) the increasing public opposition to animal testing¹. This has created a large demand for difficult to obtain human parenchymal cells, including cardiomyocytes, hepatocytes and neurons. Acquisition of such terminally differentiated cell types is complicated by the fluctuating availability and inconsistent quality of source material including post-mortem samples, surgical waste, non-transplanted donor tissue and biopsies. Additionally, these cell types cannot be multiplied *in vitro* and rapidly dedifferentiate in culture, severely restricting the window of use after isolation. Permanent human cell lines of tumor origin or created through genetic engineering generally have not been able to recapitulate the functional properties of the primary cells from which they were derived, because in most cell types continuing proliferation inhibits differentiation².

Many of these drawbacks have been overcome by the establishment of human embryonic stem cell (hESC) lines³ and, more recently, of human induced pluripotent stem cell (hiPSC) lines^{4,5}, in conjunction with the development of new methods to derive various differentiated cell types from them. As a result, human (pluripotent) stem cell-based 2- and 3-dimensional multicellular *in vitro* models including organoids⁶ are rapidly gaining popularity for human disease modeling, target identification, drug development and therapeutic testing. A particularly attractive feature of hiPSCs is the ease with which they can be generated from individual patients allowing the development of patient-specific disease models, thereby creating unique opportunities for personalized medicine. Despite the many advantages of human (pluripotent) stem cell-based *in vitro* models, there are still several factors that limit their application: 1) Derivation of specialized cells from human (pluripotent) stem cells is often a complex and laborious process with a variable outcome; 2) Producing large numbers of specialized cells with a high degree of phenotypic uniformity from human (pluripotent) stem cells is difficult; 3) The

differentiated progeny of human (pluripotent) stem cells typically has an immature phenotype and thus functionally differs from adult human cells.

In an attempt to address these limitations, we recently developed a monopartite lentiviral vector (LV)-based system for the conditional immortalization of primary mammalian cells^{7,8}. At the heart of this system is a recombinant simian virus 40 (SV40) large T (LT) gene, whose expression is driven by a cell type-specific promoter and can be repeatedly switched on and off by means of the tetracycline/doxycycline (dox)-controlled transcription silencer TetR-KRAB^{9,10}. In the present study, we employ this conditional immortalization to generate, for the first time, lines of human atrial myocytes (AMs) with preserved cardiomyogenic differentiation capacity. The reasons for choosing human AMs as target cells are two-fold: 1) Their highly specialized nature and specific functional properties (*i.e.* excitability and contractility), provide a stringent test for the effectiveness of our conditional cell immortalization system. 2) The rapid worldwide increase in the prevalence of atrial fibrillation (AF)¹¹, its high socioeconomic burden¹², the incomplete mechanistic understanding¹³ along with substantial translational challenges¹⁴ and the suboptimal treatment options¹⁵, have created an urgent need for a robust source of human AMs to overcome the current lack of clinically relevant (*in vitro*) models of AF¹⁶.

Transduction of human fetal AMs (hfAMs) with the TetR-KRAB-regulated LT-encoding LV resulted in the generation of 15 monoclonal cell lines designated hiAMs that rapidly proliferated in the presence of dox and differentiated into excitable and contractile cells with molecular, cellular and electrophysiological properties of AMs after dox withdrawal. These unique cell lines were used to establish the first multicellular *in vitro* AF models featuring fibrillatory activity with clinically relevant dynamics and activation frequencies, which could be terminated with traditional antiarrhythmic drugs. The development of the hiAM lines provides proof-of-concept of a versatile new method to produce, in a simple and rapid manner, massive numbers of authentic human cells for comprehensive disease modeling.

RESULTS

Generation and selection of hiAMs

To conditionally immortalize human atrial cardiomyocytes, human fetal atrial tissue (gestational age 18 weeks) was dissociated. The resulting cell suspension was transduced with LV particles containing a dox-inducible SV40 LT expression unit driven by the strong hybrid striated muscle-specific MHCK7 promoter¹⁷, targeting the cardiomyocyte population in the atrial cell mixture (Fig. 1a, Supplementary Fig. 1). Two to three weeks after induction of SV40 LT synthesis through addition of dox and reseeding single cells at ultra-low density, proliferating colonies comprising 100-200 cells appeared (Fig. 1b). To assess whether the conditional immortalization was successful, 95 proliferating colonies were isolated, expanded and graded using predefined criteria to assess both the proliferative activity of the cells in the presence of dox and their ability to reacquire the differentiated properties of AMs following dox removal (Fig. 1c, Supplementary Fig. 1). To meet these criteria, the monoclonal lines should display the following properties: 1) proliferate well in the presence of dox (> 15 population doublings [PDs] with a doubling time < 120 h), 2) cease proliferation following dox removal and acquire a cardiomyocyte-like phase contrast appearance after 12 days of culture in differentiation medium, 3) stain negative for proliferation marker Ki-67 and positive for cardiac troponin T at 12 days after dox withdrawal and 4) generate and conduct (typical atrial) electrical impulses following cardiomyogenic differentiation in confluent monolayers (action potential [AP] duration [APD] at 80% repolarization [APD₈₀] < 300 ms and conduction velocity [CV] > 10 cm/s) (Fig. 1d,e and Supplementary Fig. 1). Fifteen of the 95 (15.8%) monoclonal lines, designated human immortalized AMs (hiAMs), adhered to all 4 predefined criteria indicating successful generation, through conditional immortalization, of the first lines of human cardiomyocytes with preserved cardiomyogenic differentiation capacity.

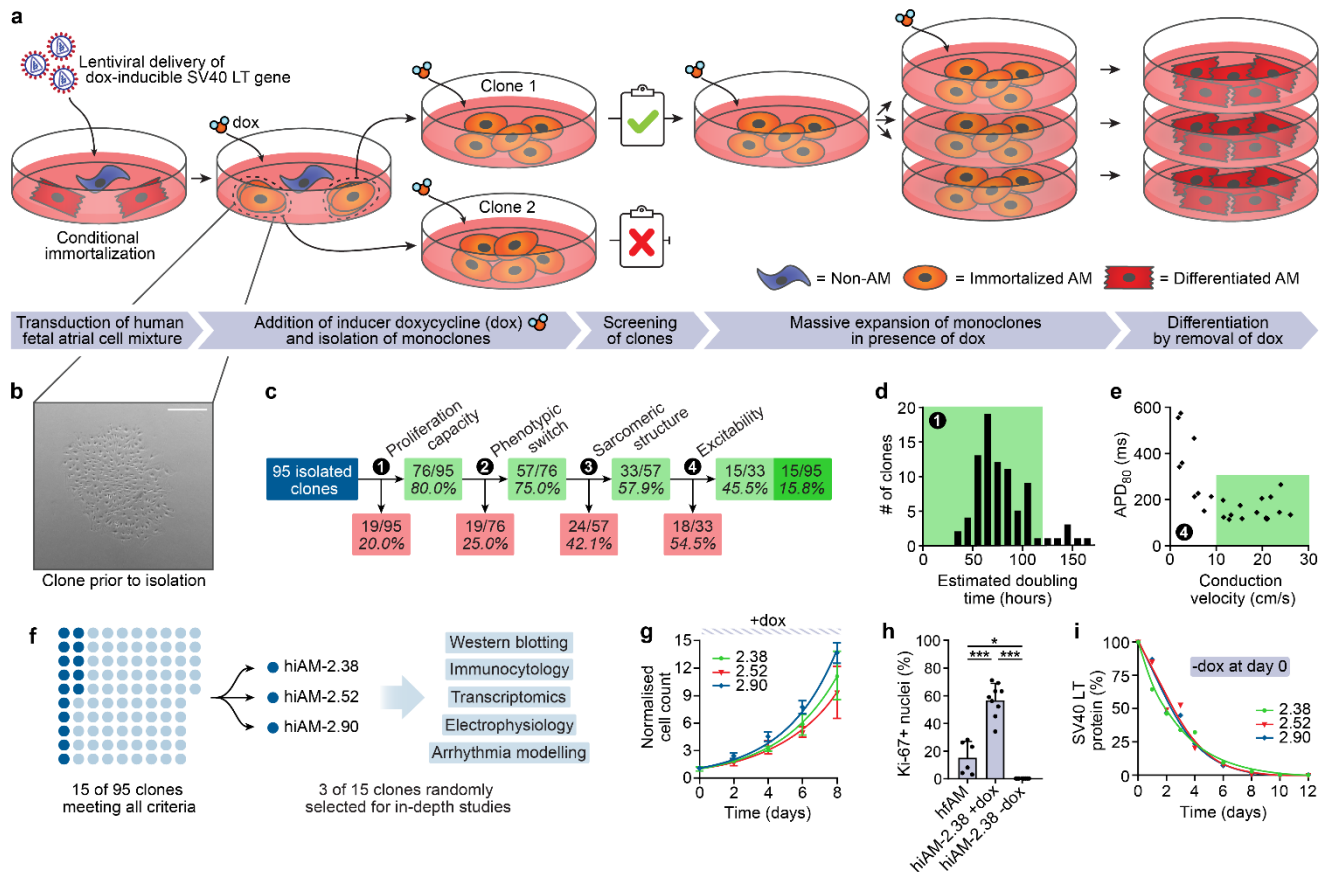


Fig. 1: Generation and selection of hiAM monoclonal cell lines. (a) Schematic overview of the conditional immortalization of hfAMs, generation and selection of hiAM monoclonal cell lines, massive hiAM expansion in the presence of dox and cardiomyogenic differentiation of hiAMs following dox removal. (b) Representative phase contrast image of a hiAM monoclonal cell culture. Scale bar, 500 μ m. (c) Flowchart of hiAM monoclonal cell line selection based on four main criteria with corresponding drop-off rates (see Supplementary Fig. 1 for additional data). (d) Estimated doubling time of isolated hiAM monoclonal cell lines based on passaging intervals. The highlighted area (doubling time ≤ 120 h) represents a pass on the first selection criterion. (e) Selection based on excitability of hiAM monoclonal cell lines using optical voltage mapping as part of the fourth selection criterion. The highlighted area represents selected monoclonal cell lines with a CV ≥ 10 cm/s and APD₈₀ ≤ 300 ms. (f) Summary of monoclonal cell line selection. hiAM clones 2.38, 2.52 and 2.90 were selected for further characterization. (g) Quantification of hiAM proliferation in the presence of dox ($n = 3$ per monoclonal cell line; error bars, SD). (h) Ki-67⁺ nuclei determined by immunocytochemistry in hfAM ($n = 2$), proliferating (+dox, $n = 3$) hiAM and differentiated (-dox, $n = 3$) hiAM cultures. Three random areas per culture were selected for quantification. n signifies independent samples/differentiations. * $P < 0.05$, *** $P < 0.001$, one-way analysis of variance with Tukey *post-hoc* analysis. (i) SV40 LT levels in proliferating hiAM-2.38, -2.52 and -2.90 measured by western blotting over 12 days of differentiation following removal of dox at day 0 ($n = 1$ per monoclonal cell line).

Characterization of hiAMs during proliferation and after differentiation

Three of the 15 hiAM clones (*i.e.* hiAM clones 2.38, 2.52 and 2.90) were randomly selected for in-depth characterization (Fig. 1f). The doubling time of the 3 selected hiAM clones in the presence of dox, was 55 ± 5 h (Fig. 1g). Immunocytochemistry confirmed a significant increase of proliferation marker Ki-67-positive nuclei in proliferating hiAMs compared to freshly isolated hfAMs (56.9 ± 13.2 vs. $15.3 \pm 11.6\%$, $P < 0.001$, Fig. 1h), consistent with the limited mitotic activity of human cardiomyocytes in the second semester of gestation¹⁸. hiAMs could be expanded for at least 50 PDs without a noticeable reduction in proliferation rate, resulting in \geq quadrillion-fold cell multiplication. Dox omission in the culture medium resulted in a strong (*i.e.* > 2000 -fold) reduction of the SV40 LT level in hiAMs over the course of 12 days, as determined by western blotting (Fig. 1i). At the same time, hiAMs no longer displayed any Ki-67-positive nuclei ($0.0 \pm 0.0\%$, Fig. 1h).

The 12-day transition from a proliferating to a differentiated hiAM, which is simply initiated by the removal of dox and a change from proliferation to differentiation medium, was accompanied by the reappearance of spontaneous synchronous contractions similar to those observed in freshly isolated hfAMs (Supplementary Video 1). Immunostaining for the sarcomeric proteins α -actinin, cardiac troponin T and the atrial isoform of myosin regulatory light chain 2 (MLC2a), showed that the highly organized sarcomeres observed in hfAMs were lost following conditional immortalization and induction of proliferation, but reappeared when hiAMs were growth-arrested by dox withdrawal and allowed to redifferentiate for 12 days (Fig. 2a, Supplementary Fig. 2). Also gap junctional protein connexin-43, which was concentrated at cell-cell interfaces in hfAMs, disappeared when proliferation was induced and formed again neatly organized cell-cell connections following hiAM differentiation. At all stages, hfAMs and hiAMs stained negative for the ventricular isoform of myosin regulatory light chain 2 (MLC2v), corroborating their atrial origin and specificity.

We next performed RNA-sequencing to study the transcriptome of proliferating and cardiomyogenically differentiated hiAMs (Fig. 2b). Principal component analysis and heatmap of global gene expression data illustrated a clear separation between the transcriptomes of the proliferating (D0) and differentiated (D12) hiAM clones (Fig. 2c, Supplementary Fig. 3). Grouped comparison

revealed differential expression of 6078 genes, of which 2652 were downregulated and 3426 were upregulated when transitioning from proliferation to differentiation (\log_2 fold-change > 1 and false discovery rate [FDR]-corrected $P < 0.001$, Supplementary Data 1). Differential gene expression of individual clones showed a large overlap (Fig. 2d). Downregulated genes standing out (including *MKI67*, *AURKB*, *CDK1*, *CCNA2* and *POLE*) appeared to be closely involved with cell proliferation, whereas upregulated genes (such as *ACTN2*, *MYH6*, *KCNJ2*, *CACNA1C* and *GJA5*) were associated with a differentiated AM phenotype (Fig. 2e). These observations were confirmed by gene ontology (GO) analysis of the up- and down-regulated genes (Fig. 2f, Supplementary Fig. 4). GO terms enriched during hiAM proliferation were mainly related to DNA replication and cell division, whereas the most enriched GO terms post-differentiation were involved in myofibrillogenesis, energy metabolism and cardiac muscle contraction. The differential expression levels of atrial and ventricular marker genes, such as *MYL7/MYL2* (19669.6 vs. 0.2 transcripts per million [TPM]), *MYH6/MYH7* (1126.4 vs. 15.6 TPM) and *HEY1/HEY2* (0.68 vs. 0.00 TPM), as well as the high abundance of *NPPA* transcripts (8494.6 TPM), further confirmed the atrial phenotype of hiAMs (Supplementary Fig. 5). Differentiated hiAMs also expressed ion channel genes known to underlie atrium-specific ion currents including *KCNA5* (ultrarapid delayed rectifier K^+ current [I_{Kur}]), *KCNJ3/KCNJ5* (acetylcholine-sensitive K^+ current [$I_{K,ACh}$]), *KCNN2/KCNN3* (small-conductance Ca^{2+} -activated K^+ current [I_{SK}]) and *KCNK1/KCNK3* (two-pore domain K^+ current [I_{K2P}]) (Supplementary Fig. 5). Collectively, these results demonstrate that the conditional immortalization by TetR-KRAB-regulated SV40 LT gene expression allows hfAMs to effectively switch between proliferative and differentiated states, which could not be achieved with permanent immortalization (Supplementary Fig. 6).

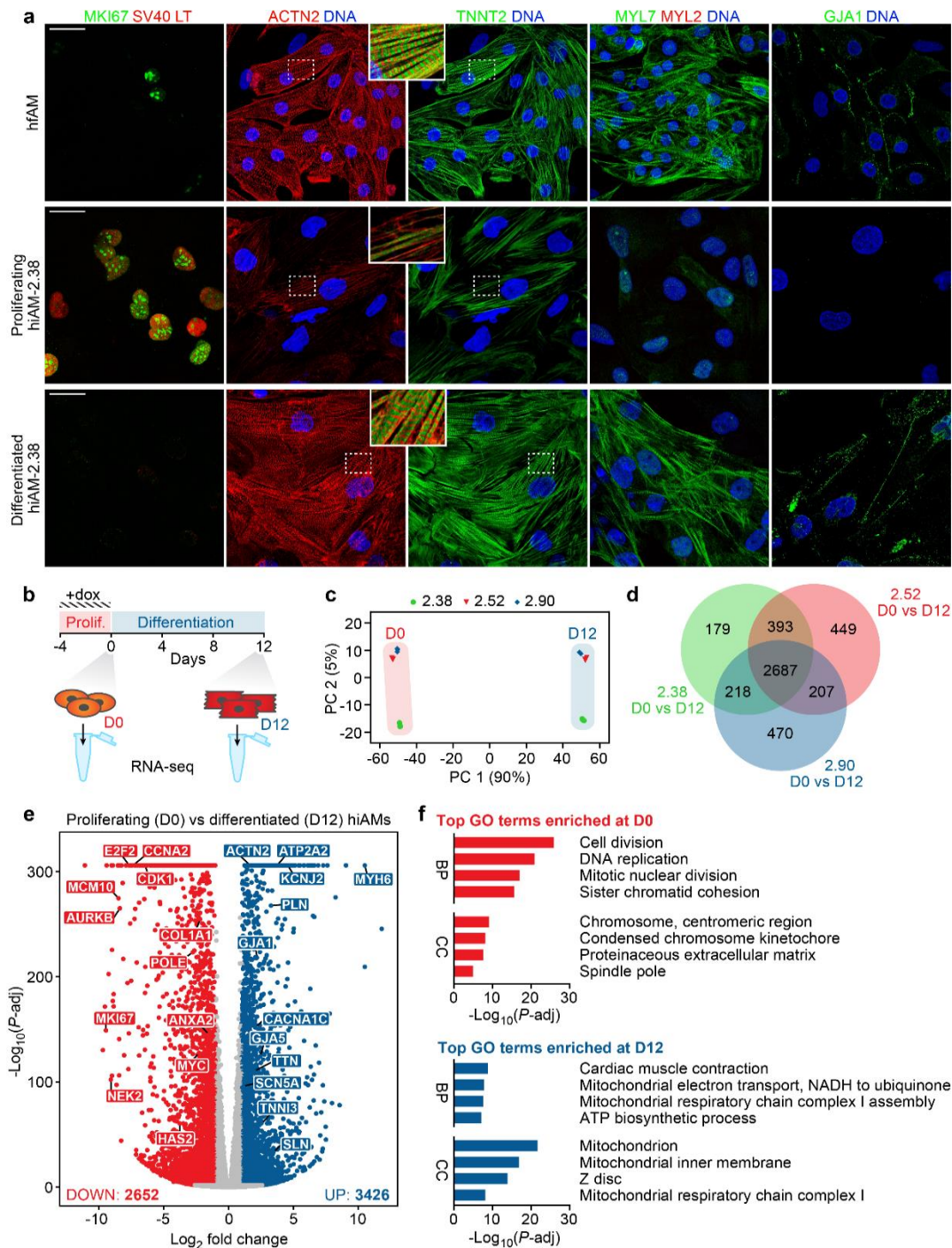


Fig. 2: Characterization of the hiAM phenotype during proliferation and after 12 days of differentiation. (a) Immunostaining of hfAM and of proliferating and differentiated hiAM-2.38 for Ki-67 (MKI67), SV40 LT, α -actinin (ACTN2), cardiac muscle troponin T (TNNT2), the atrial and ventricular isoform of myosin regulatory light chain 2 (MYL7 and MYL2, respectively) and connexin-43 (GJA1). Scale bar, 25 μ m. (b) Schematic representation of sample collection timeline for RNA-sequencing. (c) Principal component (PC) analysis of global gene expression data ($n = 3$ biological replicates per time point and hiAM clone). (d) Venn diagram of differentially expressed genes (DEGs) between proliferating (D0) and differentiated (D12) hiAM-2.38, -2.52 and -2.90. Genes with > 1 TPM at D0 or D12, an absolute \log_2 fold-change > 1 and an FDR-corrected $P < 0.001$ are shown. (e) Volcano plot of gene expression in proliferating versus differentiated hiAMs (grouped analysis of hiAM clones 2.38, 2.52 and 2.90). Selected genes of interest are labeled. Please note that due to filtering applied in the comparison of the individual clones, the number of DEGs is lower than in the grouped analysis. (f) Top 4 biological process (BP) and cellular component (CC) GO terms enriched in proliferating (D0) and differentiated (D12) hiAMs (see Supplementary Fig. 5 for all enriched GO terms).

Electrophysiological properties of differentiated hiAMs

The electrophysiological properties of cardiomyogenically differentiated hiAMs were first studied by single-cell patch-clamp analysis. Comparing the AP properties of hfAMs ($n = 6$) and differentiated hiAM-2.38 ($n = 21$) during 1-Hz stimulation revealed a slightly more negative resting membrane potential (RMP: -74.4 ± 1.0 vs. -81.9 ± 1.1 mV, $P = 0.002$) and higher maximal AP amplitude (APA_{\max} : 85.2 ± 5.9 vs. 105.5 ± 2.9 mV, $P = 0.002$) in the differentiated hiAM-2.38 (mean \pm standard error of the mean [SEM], unpaired t -test, Fig. 3a,b). AP plateau amplitude (APA_{plat} : 47.0 ± 4.0 vs. 62.6 ± 5.5 mV, $P = 0.14$), maximum AP upstroke velocity (V_{\max} : 130.2 ± 27.9 vs. 171.9 ± 26.1 V/s, $P = 0.41$) and APD at 20%, 50% and 90% of repolarisation (APD_{20} : 6 ± 2 vs. 12 ± 3 ms, $P = 0.22$; APD_{50} : 37 ± 15 vs. 36 ± 8 ms, $P = 0.97$; APD_{90} : 152 ± 27 vs. 152 ± 17.0 ms, $P = 0.99$) did not significantly differ between the two groups (mean \pm SEM, unpaired t -test, Fig. 3a,b, Supplementary Table 1). Also, differentiated hiAM-2.52 and hiAM-2.90 displayed similar AP characteristics when compared to hfAMs (Supplementary Fig. 7, Supplementary Table 1). Thus, the AP properties of differentiated hiAMs strongly resemble those of primary hfAMs.

Next, we assessed the conduction of APs in multicellular preparations by optical voltage mapping. Upon 1-Hz electrical point stimulation, cell layers (2-cm^2) of hiAM-2.38 displayed homogeneous conduction of APs (Fig. 3c,d) with a CV of 24.4 ± 2.3 cm/s and APD_{80} of 136 ± 12 ms ($n = 28$, Fig. 3e), with APD restitution occurring at high activation frequencies (Fig. 3f). Optical voltage mapping of hiAM-2.52 ($n = 19$) and hiAM-2.90 ($n = 21$) also showed homogeneous conduction of APs at speeds of 19.4 ± 2.0 cm/s and 11.9 ± 2.0 cm/s and with an APD_{80} of 129 ± 15 ms and 103 ± 9 ms, respectively, Supplementary Fig. 7). Since confluent monocultures of hfAMs could not be established because of the limited availability of cells and the difficulty to remove the large percentage of non-cardiomyocytes from the starting material, we used hESC-derived atrial cardiomyocytes (hESC-AMs) for comparison. Due to limited production capacity of phenotypically homogenous hESC-AM populations, this comparison was performed in confluent 1-cm^2 cell layers. Conduction in hESC-AM layers appeared more heterogeneous and was > 10 -fold slower compared with hiAM-2.38 layers of the same size (2.1 ± 0.4 vs. 23.6 ± 0.9 cm/s, $P < 0.001$, both $n = 7$, Fig. 3g-i Supplementary Video 2). In

terms of optical AP characteristics, the optical upstroke time was longer in hESC-AMs compared with hiAM-2.38 (28 ± 6 vs. 12 ± 1 ms, $P < 0.001$, $n = 6$ and 7 , respectively) while APD_{80} did not statistically differ between hESC-AMs and hiAMs (121 ± 41 vs. 155 ± 10 ms, $P = 0.06$, both $n = 7$).

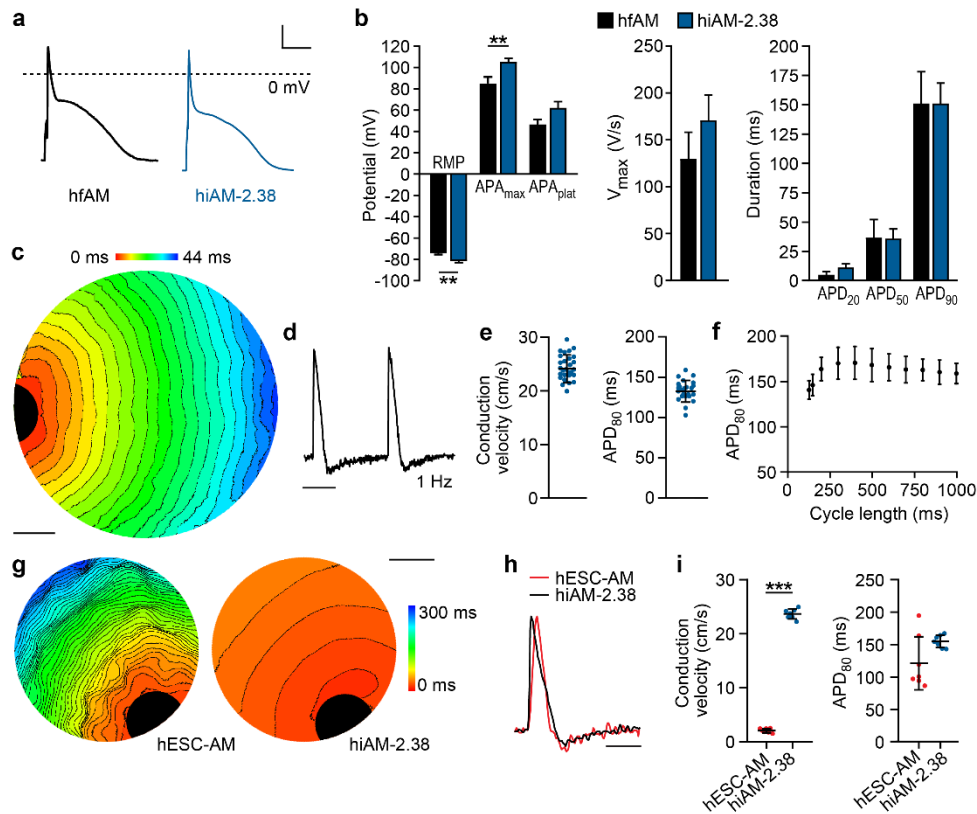


Fig. 3: Electrophysiological characteristics of differentiated hiAMs. (a) Representative AP traces and (b) mean AP parameters of single hfAMs ($n = 6$ cells from 2 independent preparations) and single differentiated hiAM-2.38 ($n = 21$ cells from 6 independent differentiations) during 1-Hz electrical stimulation. Scale bars in (a) $x = 50$ ms, $y = 20$ mV. The dotted line in (a) indicates the zero mV level. Error bars indicate standard error of the mean. $**P < 0.01$, unpaired t -test. (c-f) Optical voltage mapping of confluent layers of differentiated hiAMs in a 24-well format following 1-Hz electrical point stimulation. (c) Representative activation map of hiAM layer. Isochrones, 2 ms. Scale bar, 2 mm. (d) Representative optical voltage trace of hiAMs from (c). Scale bar, 500 ms. (e) Mean CV and APD_{80} in confluent hiAM layers ($n = 28$ from 8 independent differentiations). Error bars indicate SD. (f) APD restitution curve of hiAM-2.38 ($n = 10$ from 2 independent differentiations). Error bars indicate SD. (g-h) Optical voltage mapping of confluent hESC-AM and differentiated hiAM-2.38 layers in a 48-well format. (g) Representative activation maps of hESC-AM and hiAM-2.38 layers. Isochrones, 6 ms. Scale bar, 2 mm. (h) Representative optical voltage traces from hESC-AMs and hiAMs of (g). Scale bar, 250 ms. (i) Mean CV and APD_{80} during 1-Hz electrical stimulation in hESC-AM ($n = 7$ from 3 independent differentiations) and differentiated hiAM ($n = 7$ from 2 independent differentiations) layers. Error bars indicate SD. $***P < 0.001$, unpaired t -test.

Robustness of hiAM differentiation

Further, we assessed the robustness of hiAM differentiation, being paramount for standardized cell lines. First, we found that massive expansion of hiAMs did not jeopardize their cardiomyogenic differentiation potential. Comparison of optical voltage mapping data of hiAM-2.38 that had undergone different PDs (between 28 and 46) before cardiomyogenic differentiation, revealed no significant change in average CV or APD₈₀ ($n = 111$, $P = 0.96$ and $P = 0.15$, respectively, Fig. 4a, Supplementary Fig. 8). Also, no variation in structural characteristics as assessed by immunostaining for α -actinin and cardiac troponin T was observed over this broad range of PDs (Supplementary Fig. 8). Next, we tested whether hard-to-control variations in the culture medium, such as the variable composition of fetal bovine serum (FBS)¹⁹, would affect cardiomyogenic differentiation. The CV of hiAM cultures differentiated with four different sources of FBS did not significantly differ ($P = 0.28$, Fig. 4b). Similarly, no effect of FBS type on APD₈₀ was found, except that the premium FBS from USA origin had a minimal shortening effect on APD₈₀ as compared to the FBS from South America, New Zealand and Brazil ($P = 0.01$, $P = 0.003$ and $P = 0.001$, respectively, Fig. 4b). Finally, we investigated whether cryopreservation of differentiated hiAMs (in addition to cryopreservation of proliferating hiAMs) would be feasible. Thawing of hiAMs that had been cryopreserved at day 8 of differentiation, *i.e.* just before they exhibit contractions, resulted in $91.9 \pm 1.6\%$ of viable cells and an attachment efficiency of $70.4 \pm 5.2\%$ ($n = 3$ batches of $n = 3$ vials, Fig. 4c). Following 6 additional days of culture in differentiation medium to complete cardiomyogenesis, the hiAM layers ($n = 8$) did not show significant differences in electrophysiological characteristics when compared to control layers established with hiAMs that had not been cryopreserved in a partially differentiated state ($n = 9$; CV: 21.7 ± 2.2 vs. 23.0 ± 1.5 cm/s; APD₈₀: 138 ± 21 vs. 145 ± 22 ms, $P = 0.17$ and $P = 0.47$, respectively, Fig. 4d). Together, these data demonstrate robust hiAM differentiation irrespective of passage history, culture conditions or intermediate cryopreservation.

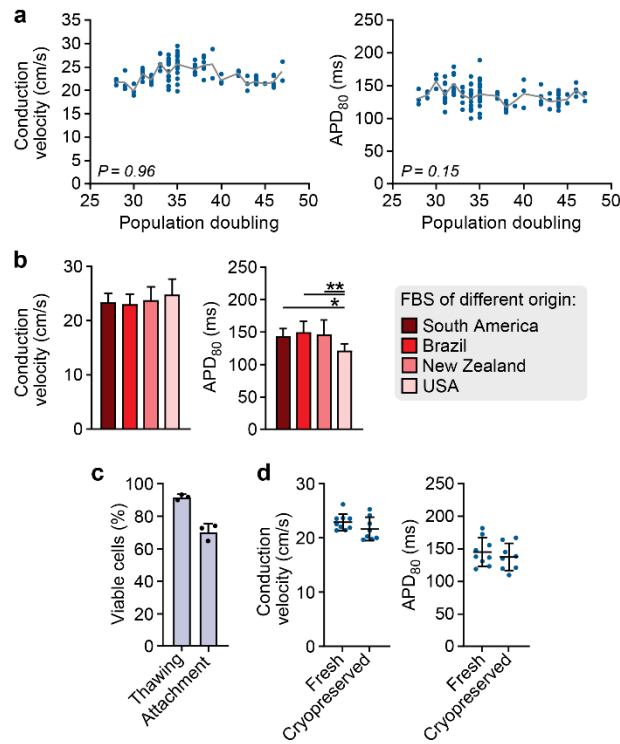


Fig. 4: Robustness and effect of cryopreservation on hiAM differentiation capacity. (a) CV and APD₈₀ of hiAM-2.38 layers measured using optical voltage mapping over a broad range of population doublings ($n = 111$). Stability of mean CV and APD₈₀ at various PDs was tested using the Pearson correlation coefficient. (b) Electrophysiological characteristics of hiAM-2.38 layers following differentiation using FBS of various origins and suppliers: South America (standard serum, S1860, Biowest), Brazil (10270098, Thermo Fisher Scientific), New Zealand (A3160901, Thermo Fisher Scientific) and USA (Premium FBS, 16000036, Thermo Fisher Scientific; $n = 13$ per group from 3 independent differentiations). $*P < 0.05$, $**P < 0.01$, one-way analysis of variance with Tukey *post-hoc* analysis. (c) Viability (determined by the Trypan Blue dye exclusion test) and attachment efficiency after thawing of hiAMs that had been cryopreserved at day 8 of differentiation ($n = 3$ batches each comprising 3 vials with 10^6 hiAMs per vial). (d) Electrophysiological characteristics using optical voltage mapping of freshly differentiated hiAM-2.38 ($n = 9$ from 3 independent differentiations) versus cryopreserved differentiated hiAM-2.38 layers ($n = 8$ from 3 independent differentiations). (b-d) Error bars indicate SD.

hiAMs as atrial arrhythmia model

We next investigated the suitability of hiAMs for AF modeling. As induction of reentry in hiAM layers was not feasible in the 2-cm² format and the average area of reentrant circuits in human AF is ~3 cm²^{20,21}, we used 10-cm² confluent hiAM layers to provide space for multiple reentrant circuits. hESC-AM layers of 1 cm² were included for comparison, because of the aforementioned difficulty to establish larger confluent monolayers of these cells. Upon high-frequency electrical point stimulation, arrhythmic activity with varying degrees of complexity could be induced in both 1-cm² hESC-AM and 10-cm² hiAM layers (Fig. 5a,b, Supplementary Video 3). Reentrant activity induced in hESC-AM layers had an average activation frequency of 3.0 ± 0.8 Hz ($n = 16$), which was consistent with previous reports of arrhythmic hESC-AM layers²². In hiAM-2.38 layers, however, the average activation frequency was significantly higher (7.5 ± 1.0 Hz, $n = 56$, $P < 0.001$, Fig. 5c). Also in hiAM-2.52 and hiAM-2.90 layers, reentrant activity with high activation frequencies could be induced (7.2 ± 0.8 and 7.9 ± 0.6 Hz, $n = 11$ and $n = 12$, respectively, Supplementary Fig. 9). Interestingly, these activation frequencies very closely resemble those previously measured in the clinic in AF patients²³⁻²⁵. As expected from the faster CV in hiAM layers, reentrant circuit wavelength was greater in hiAM-2.38 layers than in hESC-AM layers (17.0 ± 3.2 vs. 2.4 ± 0.8 mm, $P < 0.001$, $n = 56$ and $n = 16$, respectively, Fig. 5d). As a result, the arrhythmia complexity (expressed as number of reentrant circuits per cm²) was higher in hESC-AM layers compared to hiAM-2.38 layers (1.65 ± 0.77 vs. 0.14 ± 0.07 , $P < 0.001$, $n = 16$ and $n = 56$, respectively, Fig. 5e, Supplementary Video 4). Similar data were obtained in arrhythmic hiAM-2.52 and hiAM-2.90 layers (Supplementary Fig. 9). Moreover, in hESC-AM layers, the cycle length of reentrant circuits was much longer than the baseline APD₈₀, whereas in hiAMs these two parameters were very similar (Fig. 5f and Supplementary Fig. 9). Reentrant circuits in hESC-AMs displayed a large temporal excitable gap compared to nearly no gap in hiAMs (hESC-AM: 210 ± 71 ms vs. hiAM-2.38: 28 ± 10 ms, $P < 0.001$, $n = 16$ and $n = 56$, respectively, Supplementary Fig. 9), which suggests that the slow CV in hESC-AM layers might be responsible for the low activation frequencies. Overall, hiAM monolayers better recapitulate the dynamics of human AF than hESC-AM monolayers.

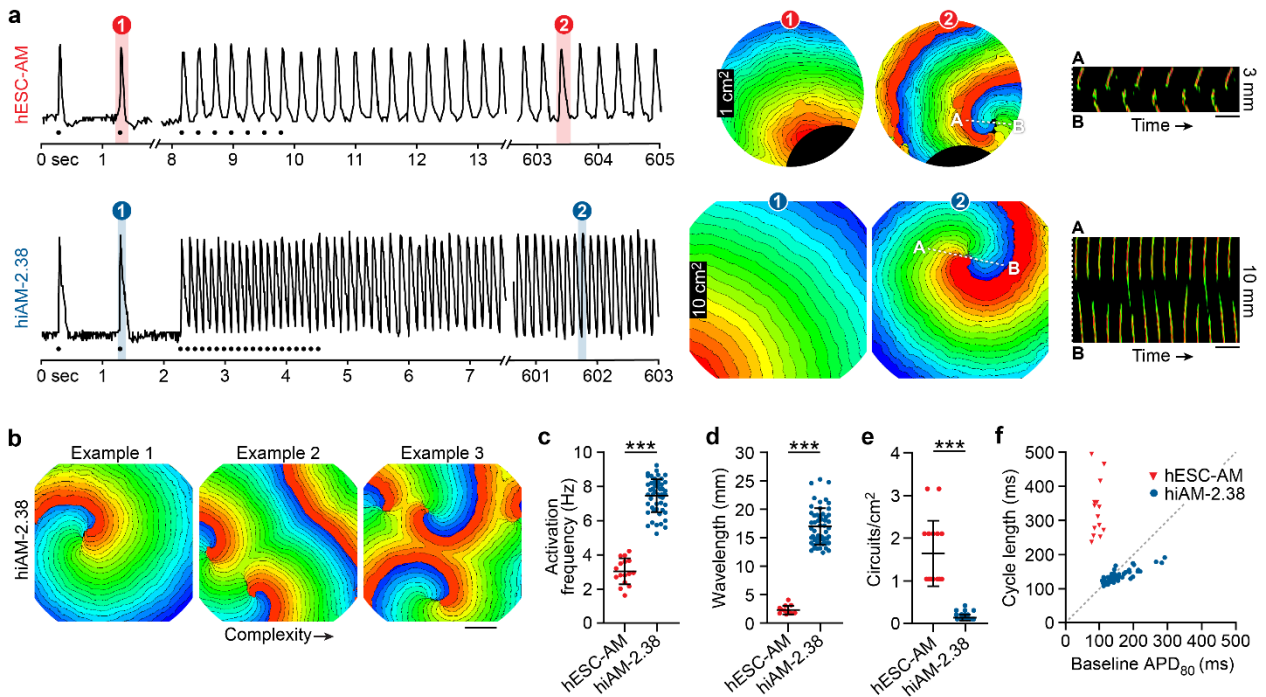


Fig. 5: hESC-AM- and hiAM-based atrial arrhythmia models. (a) Optical voltage traces of reentrant circuit induction by high frequency electrical pacing in 1-cm² hESC-AM and 10-cm² differentiated hiAM cultures (left). Corresponding activation maps before and after arrhythmia induction (middle). Line scan analysis between points A and B assessing reentrant circuit stability (right). Dots above the axes represent time points of electrical stimulation. Isochrones, 12 ms (hESC-AM), 6 ms (hiAM). Scale bar, 250 ms. (b) Example of three 10-cm² hiAM-2.38 cultures following induction of reentrant activity of increasing complexity, *i.e.* with an increasing number of reentrant circuits. Isochrones, 6 ms. Scale bar, 5 mm. (c) Mean activation frequency of hESC-AM and hiAM cultures following induction of reentrant circuits. (d) Mean wavelength of reentrant circuits. (e) Arrhythmia complexity following stabilization expressed as number of reentrant circuits per cm². (f) Correlation between baseline APD₈₀ and cycle length of induced reentrant circuits in hESC-AM and hiAM cultures. (c-e) Error bars indicate SD. *** $P < 0.001$, unpaired t -test. (c-f) hESC-AM: $n = 16$ from 7 independent cultures, hiAM-2.38: $n = 56$ independent cultures.

Effects of traditional antiarrhythmic drugs in hiAM-based AF model

The applicability of the hiAM-based AF model to study pharmacological interventions was tested using sotalol and flecainide, two antiarrhythmic drugs commonly used for rhythm control in AF patients²⁶⁻²⁸. Dimethylsulfoxide (DMSO), which served as solvent/vehicle for flecainide, did not affect the CV or APD in hiAM-2.38 layers subjected to 1-Hz electrical point stimulation. Increasing concentrations of sotalol had also no effect on CV, but did dose-dependently increase the APD₈₀ (Fig. 6a and Supplementary Fig. 10), as would be expected by its strong inhibitory effect on the rapid delayed rectifier K⁺ current (I_{Kr})²⁹. Flecainide, which mainly inhibits the Na⁺ current (I_{Na}) and I_{Kr}³⁰, decreased the CV and prolonged the APD₈₀ in a dose-dependent matter. For each compound, three incremental doses were selected (DMSO: 0.01, 0.03 and 0.1%; Sotalol: 3, 10 and 30 μM; Flecainide 1, 3 and 10 μM), including clinically relevant concentrations (Fig. 6b).

Following the induction of stable reentry in hiAM-2.38 cultures, slow infusion of DMSO rarely resulted in termination of reentrant activity (Fig. 6c). Within 10 min of infusion, the rate of reentrant activity termination was 0/9 (0%) for 0.01% DMSO, 1/9 (11%) for 0.03% DMSO and 0/10 (0%) for 0.1% of DMSO (Fig. 6d). DMSO also did not significantly alter the activation frequency, with the exception of the 0.01% dose which slightly reduced the frequency (7.6 ± 1.1 to 6.9 ± 1.7 Hz, $P = 0.03$, Fig. 6e). Sotalol infusion resulted in sporadic termination of reentrant activity (2/9 [22%], 0/10 [0%] and 2/10 [20%] for 3, 10 and 30 μM, respectively), although for none of these doses termination rates significantly differed from those caused by DMSO treatment. The activation frequency, however, was significantly reduced for all sotalol concentrations in a dose-dependent manner (3 μM: 7.4 ± 0.9 to 7.1 ± 1.0 Hz; 10 μM: 7.4 ± 1.1 to 5.6 ± 1.1 Hz; 30 μM: 7.4 ± 1.1 to 5.4 ± 0.9 Hz, all $P < 0.001$). Finally, infusion of flecainide did result in frequent termination at the two highest doses (0/8 [0%], 3/9 [33%, $P < 0.04$] and 6/8 [75%, $P < 0.001$] for 1, 3 and 10 μM, respectively). Also, infusion of flecainide significantly reduced the activation frequency in a dose-dependent manner (1 μM: 7.8 ± 1.0 to 6.1 ± 1.4 Hz; 3 μM: 7.2 ± 1.6 to 4.6 ± 2.7 Hz; 10 μM: 6.8 ± 1.0 to 2.7 ± 2.0 Hz, all $P < 0.001$). These observations were also confirmed in hiAM-2.52 and hiAM-2.90 cultures (Supplementary Fig. 11). For these clones, 0.1% DMSO did not terminate any reentrant activity (hiAM-2.52: 0/8 [0%]; hiAM-2.90: 0/8 [0%]),

whereas 10 μM flecainide resulted in frequent reentry termination (hiAM-2.52: 7/8 [88%, $P < 0.001$]; hiAM-2.90: 5/8 [63%, $P < 0.001$]). Thus, using the hiAM-based AF model, we were able to recapitulate the effects exerted by common antiarrhythmic drugs in AF patients at clinically relevant activation frequencies (Supplementary Video 5).

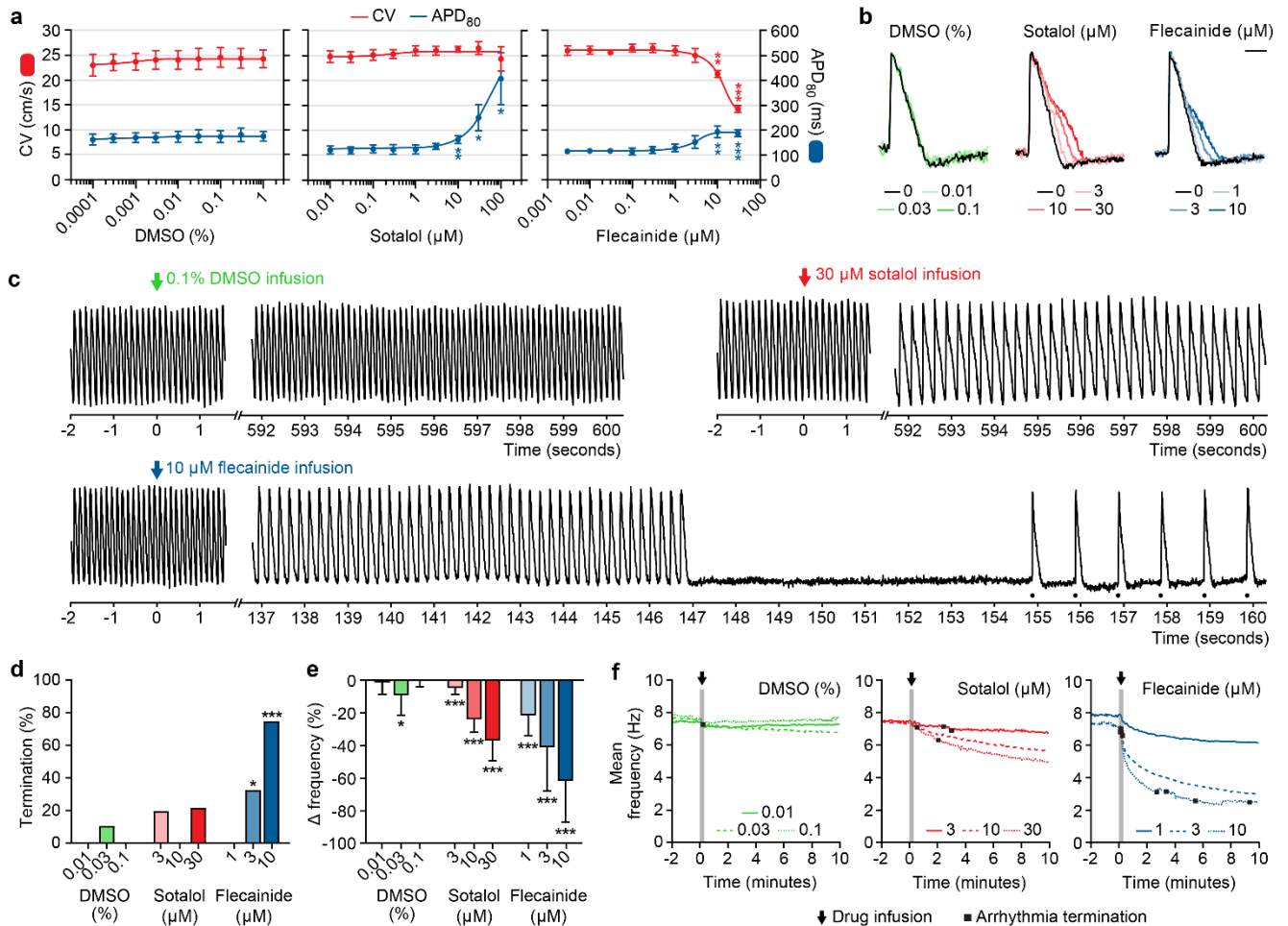


Fig. 6: Effects of antiarrhythmic drugs in the hiAM-based atrial arrhythmia model. (a) Effects of various concentrations of DMSO (as control condition), sotalol or flecainide on CV (red, left axis) and APD₈₀ (blue, right axis) in differentiated 2-cm² hiAM-2.38 cultures ($n = 5$ cultures for each condition). Repeated measured analysis of variance with Tukey *post-hoc* analysis. (b) Representative optical voltage traces of differentiated hiAM-2.38 in the presence of various concentrations of DMSO, sotalol or flecainide. Scale bar, 100 ms. (c) Representative optical voltage traces of arrhythmic hiAM-2.38 cultures before and after infusion of DMSO (0.1%), sotalol (30 μM) or flecainide (10 μM). Dots above the lower axis represent time points of electrical stimulation. (d) Rate of reentrant circuit termination in arrhythmic hiAM-2.38 cultures 10 min after infusion of DMSO, sotalol or flecainide. The termination rates at the different sotalol and flecainide concentrations were compared with the termination rate of the combined DMSO concentrations using the Chi-square test. (e) Change in activation frequency in arrhythmic hiAM-2.38 cultures following DMSO, sotalol or flecainide infusion (baseline compared to 10 min after infusion or prior to termination). Paired *t*-test. (f) Continuous monitoring of mean activation frequency in arrhythmic hiAM-2.38 cultures prior to and after infusion of compounds at various concentrations. (d-f) $n = 8-10$ for each dose, from 57 independent cultures. (a, d, e) Error bars indicate SD. * $P < 0.05$, ** $P < 0.01$, *** $P < 0.001$.

DISCUSSION

Preclinical biomedical research across academia and industry has created a large demand for difficult to obtain human parenchymal cells to increase pathophysiological insight and develop novel therapeutics. Although recent progress in human pluripotent stem cell (hPSC) technology has greatly advanced the development of human disease models, several challenges remain regarding their scalability, representativeness and reproducibility. To address these issues, we developed a LV-based method for the conditional immortalization of primary mammalian cells. In this study, we describe the generation of standardized lines of human AMs with preserved cardiomyogenic differentiation capacity as a demonstration of the efficacy of this method. These so-called hiAM lines display strict control over proliferation and differentiation, allowing massive (*i.e.* quadrillion-fold) expansion followed by differentiation towards fully functional (*i.e.* excitable and contractile) human AMs. The generation of the first differentiation-competent human cardiomyocyte lines enabled the creation of human AF models that, for the first time, feature fibrillatory activity at clinically relevant frequencies, which could be terminated using antiarrhythmic drugs used in clinical practice.

The development of human cardiac muscle cell lines with preserved cardiomyogenic differentiation capacity has been the scope of multiple studies over the last decades^{31,32}. Thus far, human cardiomyocyte lines failed to recapitulate the structural and functional characteristics of the primary cells from which they were derived. Here, we show that this shortcoming can be overcome by imposing stringent control over SV40 LT expression in the target cells. The resulting hiAM lines allow straightforward production of contractile and excitable AMs in quantities not conceivable heretofore (*e.g.* one hiAM line can generate the number of cardiomyocytes present in 100,000 human adult hearts). Due to the monoclonal nature of hiAM lines and the high efficiency with which the cells undergo cardiomyogenic differentiation, pure populations of human atrial cardiomyocytes can be produced with great ease. This provides a clear advantage over derivation of AMs from hPSCs, which is a rather laborious and time-consuming multiphase process that generally includes a purification step^{33,34} to select against the non-AMs remaining with current differentiation protocols^{22,35,36}. Also, differentiation completely abolishes proliferation of hiAMs while hPSC-derived cardiomyocytes still display some

residual mitotic activity^{37,38}. Moreover, hPSC-AMs from different studies have a non-physiological average RMP of approximately -56 mV, reflecting their immature electrophysiological phenotype^{22,35,36,39}. Differentiated hiAMs, on the other hand, display an average RMP of -79 mV, which is well within the -70 to -85 mV range reported for human native AMs⁴⁰⁻⁴². The depolarized membranes of hPSC-AMs likely contribute to the slow AP propagation observed in confluent 2/3D cultures of these cells^{22,43,44}. Above -60 mV, a considerable fraction of Na⁺ channels becomes inactivated, resulting in a decrease of AP upstroke velocity and a consequential reduction of CV. Although the CV in hiAM layers is significantly faster than in layers of hPSC-AMs (up to 30 cm/s *vs.* up to 2.5 cm/s), it is still slower than the 60-75 cm/s reached in human adult atrial tissue⁴⁵. This can, at least in part, be explained by the absence of anisotropic organization and neurohumoral regulation in the monolayers of differentiated hiAMs⁴⁶, providing a rationale for the future application of *in vitro* patterning technology to create cables/sheets of uniaxially aligned hiAMs and thereby increase the (longitudinal) CV in these structures along with neurohormonal stimulation.

The basic electrophysiological properties of hiAMs and hPSC-AMs also directly influence their applicability for AF modeling. Laksman *et al.*²² were the first to report induction of reentrant circuits in (non-purified) hESC-AM layers at a mean frequency of 3.2 Hz, which is very similar to the 3.0 Hz we found in our (purified) hESC-AM layers, but much lower than the 7.5 Hz in hiAM layers. For reference, activation frequencies measured in AF patients range between 6 to 8 Hz, depending on the type of AF²³⁻²⁵. When studying the influence of antiarrhythmic drugs on reentry dynamics, activation frequencies resembling clinical AF are critical because of (reverse) rate-dependent effects. For instance, I_{Na}-blocking activity of flecainide is increased at higher activation frequencies⁴⁷, which could explain why termination of reentry using 10 μM flecainide was possible in the majority of hiAM layers, while this was previously not successful in hESC-AM layers²². As our novel hiAM-based AF model displays the main electrophysiological phenomena driving AF and provides new possibilities over existing models for studies into arrhythmia dynamics and antiarrhythmic drug discovery, a future extension would be to move towards more advanced 3D *in vitro* models of AF. Atrium-like 3D tissues have recently been generated using hPSC-AMs^{44,48,49}, but due to their small size (largest dimension ≤ 5 mm) they cannot

accommodate reentrant circuits with characteristics similar to human AF. Advances in bioprinting technology have already demonstrated the feasibility of creating large and complex (cardiac) scaffolds required for tissue engineering of whole human hearts⁵⁰. The main limiting factor for the creation of such large tissue constructs to date, has been the difficulty associated with generating the hundreds of millions/billions of well-differentiated cells necessary to populate these constructs. Although a recent report has shown that this problem may at least be partially overcome by a new method allowing the expansion of hiPSC-derived ventricular myocytes³⁸, it remains to be seen whether it can also induce multiplication of hPSC-AMs. Accordingly, the extensive scalability, cost-effectiveness and robustness of hiAM differentiation might provide a new impulse to create larger human atrial constructs for disease modeling, mechanistic studies and drug screening.

The ability to generate large numbers of differentiated hiAMs in an effective and robust manner may furthermore open the possibility to use them for biopharmaceutical production of, for instance, cardiomyocyte-derived exosomes and cardiokines⁵¹. The latter property together with the monoclonal origin of hiAMs and the high controllability of their phenotype and gene expression profile, makes these cells particularly suitable for (very) high-resolution “omics” studies by obviating the need for cell selection and by providing plentiful input material. This offers new possibilities 1) to identify yet unknown factors involved in cardiomyocyte proliferation and differentiation, and 2) to find novel therapeutic targets, especially when combined with (opto)genetic, pharmaceutical, chemical or physical interventions to mimic disease states.

Although the hiAM lines have many advantages over current AM sources, their suitability for regenerative purposes is limited due to the use of an integrating LV encoding an oncoprotein (*i.e.* SV40 LT) for (conditional) immortalization, which harbors the risk of tumor formation. hiAMs may, however, still be applied in animal models to optimize cardiac cell therapy, and may help to find new leads for endogenous induction of myocardial regeneration through stimulation of cardiomyocyte proliferation *in situ*. Although the high controllability and synchronicity of the transition from proliferation to differentiation could make hiAMs an excellent model for studying the molecular mechanisms underlying this transitions, they will not fully represent the natural course of events due to the very

nature (i.e. viral oncoprotein-dependent conditional immortalized state) of the cells. In addition, the initial investment associated with the development of these cell lines, as well as the need for access to primary cardiac material, makes the conditional immortalization technique less suited than hiPSC technology for widescale patient-specific disease modeling. Still, using gene delivery or genome editing technologies, hiAM sublines with genetic modifications could easily be created, allowing studying the effects of these alterations in a highly standardized cell system. This will allow to perform comprehensive mechanistic studies mimicking the different types of atrial disease⁵² preceding AF development, allowing for the first time to determine the precise molecular signatures of the diverse atrial cardiomyopathies, fostering thereby the development of novel preventive anti-AF therapies.

In summary, the conditional immortalization of hfAMs has enabled the creation of 1) the first fully differentiation-competent lines of human cardiomyocytes and 2) human *in vitro* models of AF displaying clinically relevant features. This provides proof-of-concept of a versatile new method to produce, in a simple and rapid manner, massive numbers of authentic human cells for the development of representative human *in vitro* models for animal-free disease investigation, target identification along with drug discovery and therapeutic testing.

METHODS

Lentiviral vector (LV) production. To generate vesicular stomatitis virus G protein-pseudotyped LV.iMHCK7.LT-WT particles, near confluent monolayers of 293T cells were transfected with LV shuttle construct pLV.iMHCK7.LT-WT and the packaging plasmids psPAX2 (Addgene, plasmid number: 12260) and pLP/VSVG (Thermo Fisher Scientific) at a molar ratio of 2:1:1. pLV.iMHCK7.LT-WT is identical to pLV.iMHCK7.LT-*tsA58*⁷ except for the replacement of the coding sequence of the temperature-sensitive simian virus 40 (SV40) large T (LT) mutant *tsA58* by that of wild-type LT. The 293T cells were cultured in high-glucose Dulbecco's modified Eagle's medium (DMEM, Thermo Fisher Scientific, 41966) with 10% fetal bovine serum (FBS, Thermo Fisher Scientific). The transfection mixture, consisting of 35 µg of plasmid DNA and 105 µg of linear 25-kDa

polyethyleneimine (Polysciences) in 2 ml of 150 mM NaCl per 175-cm² cell culture flask (Greiner Bio-One), was directly added to the culture medium. Approximately 16 h later, the transfection medium was replaced by 15 ml fresh high-glucose DMEM supplemented with 5% FBS and 25 mM HEPES-NaOH (pH 7.4). At ~48 h after the start of the transfection procedure, the culture supernatants were collected, cleared from cellular debris by centrifugation at room temperature (RT) for 10 min at 3,750×g and subsequent filtration through 0.45-µm pore-sized, 33-mm diameter polyethersulfone Millex-HP syringe filters (Merck Millipore). The LV particles were further purified and concentrated by underlaying 30 ml of vector suspension in a 38.5-ml polypropylene ultracentrifuge tube (Beckman Coulter) with 5 ml of 20% (wt/vol) sucrose in phosphate-buffered saline (PBS) and subsequent centrifugation for 2 h at 4°C with slow acceleration and without braking at 15,000 revolutions per min in an SW32 rotor (Beckman Coulter). Next, the supernatants were discarded and each pellet was suspended in 500 µl of PBS-1% bovine serum albumin (Sigma-Aldrich) by overnight incubation with gentle shaking at 4°C. The concentrated vector suspension was divided on ice in 100 µl aliquots for storage at -80°C.

Isolation and culture of human fetal atrial myocytes (hfAMs). Human fetal cardiac samples were obtained during elective abortions following written informed consent. This study was conducted with approval of the institutional review board of the Leiden University Medical Center (P08.087) and in compliance with the International Code of Medical Ethics of the World Medical Association. The atria were separated from the ventricles, minced into pieces of ~1 mm² and dissociated by two successive 30-min treatments with collagenase type I (225 U/ml, Worthington Biochemical) and DNase I (20 U/ml, Sigma-Aldrich) under gentle agitation at 37°C. Cells were pelleted by centrifugation for 10 min at 160×g and RT. The supernatant was removed and cells were resuspended in Ham's F10 medium (Thermo Fisher Scientific, 11550) supplemented with 100 units/mL of penicillin and 100 µg/mL of streptomycin (Thermo Fisher Scientific), 10% heat-inactivated FBS (Thermo Fisher Scientific) and 10% heat-inactivated horse serum (Thermo Fisher Scientific). The cell suspension was transferred to uncoated Primaria culture dishes (Corning) and incubated for 75 min at 37°C in a humidified atmosphere of 95% air-5% CO₂ to allow preferential attachment of non-cardiomyocytes. Unattached

cells were filtered through a nylon cell strainer (Corning) containing evenly spaced 70- μm mesh pores and seeded for experiments. For conditional immortalization, 10^4 cells/ cm^2 were seeded in a 6-well culture plate (Corning) coated with fibronectin from bovine plasma (100 $\mu\text{g}/\text{mL}$, Sigma-Aldrich). For immunocytochemistry and patch-clamping, respectively 5×10^4 and 2.5×10^4 cells/ cm^2 were seeded on fibronectin-coated glass coverslips in 24-well plates (Corning).

Conditional immortalization and selection of hiAM monoclonal cell lines. The human fetal atrial cell mixture was transduced with 2.5 μl of concentrated LV.iMHCK7.SV40-LT-WT stock (*i.e.* the vector yield of 1.65×10^5 producer cells), following two days of recovery. Three days following transduction, the culture medium was changed to hiAM proliferation medium, consisting of hiBASE medium (<https://hartlongcentrum.nl/hiMedia>), 2% FBS (Biowest), 100 units/mL of penicillin and 100 $\mu\text{g}/\text{mL}$ of streptomycin (Thermo Fisher Scientific) supplemented with 100 ng/ml dox (Sigma-Aldrich) to induce SV40 LT expression. After the observation of cell proliferation, cells were detached using Accutase (BD Biosciences) and plated at a density of 10 cells/ cm^2 in 145-mm diameter culture dishes (Greiner Bio-One) in the presence of hiAM proliferation medium. These dishes were maintained for 2-3 weeks at 37°C in a humidified atmosphere of 95% air-5% CO_2 until colonies of 100-200 cells were observed. Individual colonies were then isolated with the aid of glass cloning cylinders (\varnothing 6 mm, Corning) and treated with Accutase, after which the collection of cells inside each cylinder was transferred to single wells of a 48-well plate (Corning) in hiAM proliferation medium. Isolated colonies were given a unique number, expanded up to 10^6 cells and graded based on their proliferative and differentiation qualities. The conditional immortalization was considered successful for hiAM monoclonal cell lines that 1) when given dox-containing hiAM proliferation medium proliferated beyond 15 PDs with a PD time shorter than 120 h and 2) in the presence of dox-free hiAM differentiation medium (see below) a) stopped proliferation and gradually acquired a cardiomyocyte-like phase contrast appearance, b) lost proliferation marker Ki-67 expression and eventually consisted of > 50% of cardiac troponin T-positive cells as assessed immunocytochemistry and c) were electrically excitable with a minimal CV of 10 cm/s and maximal APD₈₀ of 300 ms following optical voltage mapping of 1- cm^2 monolayers \geq 12 days after

dox removal. All selection criteria, including corresponding drop off rates per criterium, can be found in Supplementary Fig. 1. Inquiries about the LV used for the conditional cell immortalization or about the hiAMs can be send to hiAM@hartlongcentrum.nl.

Proliferation and differentiation of hiAMs. Proliferating hiAMs were cultured in uncoated TC-treated CELLSTAR flasks (Greiner Bio-One) in the aforementioned hiAM proliferation medium. Culture medium was refreshed every 2-3 days. When confluency approached 90%, proliferating hiAMs were subjected to a 10-min treatment with Accutase at 37°C and carefully triturated into a nearly single cell suspension. Next, the cells were pelleted by centrifugation for 5 min at 160×g and room temperature and transferred in a 1:2 to 1:4 ratio to new culture flask for further multiplication, or seeded in an appropriate culture plate for cardiomyogenic differentiation. Differentiation of hiAMs was performed in culture plates coated with bovine fibronectin (100 µg/mL, Sigma-Aldrich) and initiated by changing the hiAM proliferation medium to hiAM differentiation medium, consisting of hiBASE medium (<https://hartlongcentrum.nl/hiMedia>) with 2% FBS (Biowest). Starting at day 4 of differentiation (the initiation of differentiation being day 0), hiAM differentiation medium was supplemented with hiDIFF supplement (<https://hartlongcentrum.nl/hiMedia>). Culture medium was refreshed every 2 days during differentiation. At day 12 of differentiation, the hiAMs were considered fully differentiated as at that time point CV and APD reached their plateau values. All experiments in this study were performed between day 12 to 15 after initiation of differentiation.

Proliferation assay. To assess the proliferation rates of individual clones of conditionally immortalized hfAMs (hiAMs) in the presence of doxycycline (dox), 2×10^3 cells/cm² were seeded in multiple 100-mm diameter culture dishes. At 48-h intervals following culture initiation, cells were detached using Accutase, collected in hiAM proliferation medium and mixed in a 1:1 ratio with 0.4% Trypan Blue (Sigma-Aldrich). Following brief incubation, cells were counted using a CytoSMART Cell Counter

(Corning). Population doubling times were calculated by fitting data with an exponential growth equation (GraphPad Prism, v8.0.1, GraphPad Software).

Immunocytochemistry and image quantification. hfAMs and hiAMs were seeded at a density of 8×10^4 cells/cm² on fibronectin-coated coverslips prior to fixation with 4% buffered formaldehyde (Added Pharma) for 30 min at 4°C. Cells were permeabilized by incubation with PBS/0.1% Triton X-100 (Sigma-Aldrich) for 10 min, incubated with PBS/10% normal donkey serum (NDS, Sigma-Aldrich) for 30 min to block non-specific background staining and subsequently exposed to the primary antibody in PBS containing 0.5% NDS for 2 h, all at RT. After each treatment, cells were washed three times with PBS. Secondary antibody incubation was performed in PBS containing 0.5% NDS for 45 min and nuclei were stained for 10 min with Hoechst 33342 (Invitrogen) diluted 1:1000 in PBS. For an overview of the antibodies and the dilutions at which they were applied, see Supplementary Table 2. Coverslips were mounted on StarFrost slides (VWR International) using VECTASHIELD (Vector Laboratories) and imaged with an Eclipse 80i Upright Microscope (Nikon Instruments) or TCS SP8 White Light Laser Confocal Microscope (Leica Microsystems).

Counting of Ki-67-positive nuclei on the basis of mean gray values was performed using ImageJ (v1.52a, <http://imagej.nih.gov/>). For hiAMs, all Hoechst 33342-positive nuclei were analyzed. In the case of the primary hfAMs, only the Nkx-2.5-positive nuclei were considered to avoid analysis of the non-cardiomyocytes present in the samples. The mean grey value of each nucleus was compared to a threshold to distinguish between positive and negative nuclei.

Western blotting. Adherent hiAMs were lysed on ice in RIPA buffer (50 mM Tris-HCl [pH 8.0], 150 mM NaCl, 1% NP-40, 0.5% sodium deoxycholate, 0.1% sodium dodecyl sulfate) supplemented with Roche cOmplete Mini Protease Inhibitor Cocktail (Sigma-Aldrich). The lysate was passed three times through a 30-gauge needle (BD Biosciences), centrifuged for 20 min at 4°C and 16.000×g, after which the supernatant was collected and stored at -80°C. Protein concentrations in the cleared lysates were

determined using the Pierce BCA Protein Assay Kit (Thermo Fisher Scientific). Proteins were size-fractionated in Invitrogen Bolt 10% Bis-Tris Plus gels (Thermo Fisher Scientific) and transferred to Amersham Hybond P 0.45- μ m polyvinylidene difluoride membranes (GE Healthcare) by wet electroblotting using a Bolt Mini Blot Module (Thermo Fisher Scientific). Membranes were incubated for 1 h in 2% ECL Prime blocking reagent (GE Healthcare) dissolved in Tris-based saline/0.1% Tween-20 (TBS-T). Membranes were then incubated for 1 h with the primary antibody in TBS-T/2% ECL Prime blocking reagent, washed five times with TBS-T and incubated for 1 h with corresponding horseradish peroxidase-conjugated secondary antibodies. Information about the antibodies used can be found in Supplementary Table 2. Following five washes with TBS-T, membranes were covered with SuperSignal West Femto Maximum Sensitivity Substrate (Thermo Fisher Scientific) and chemiluminescence was measured using the ChemiDoc Touch Imaging System (Bio-Rad Laboratories). SV40 LT levels were quantified with the aid of Image Lab (v6.0.1, Bio-Rad Laboratories), using levels of the housekeeping protein and loading control glyceraldehyde 3-phosphate dehydrogenase (GAPDH) for normalization purposes.

RNA isolation and RNA-sequencing. Total RNA was extracted from proliferating and differentiated hiAMs seeded at a density of 10^5 cells/cm² (10^6 cells per sample) using the RNeasy Plus Mini Kit (Qiagen) according to manufacturer's instructions. RNA-sequencing was performed by GenomeScan (Leiden, the Netherlands). Quality and integrity of the RNA were confirmed using a 2100 Bioanalyzer Instrument (Agilent Technologies), with a measured RNA quality number of 10.0 for all samples. Library preparation was performed using the NEBNext Ultra II Directional RNA Library Prep Kit for Illumina in combination with the NEBNext Poly(A) mRNA Magnetic Isolation Module (both from New England Biolabs). Sample quality and yield after cDNA synthesis and polymerase chain reaction enrichment were measured with the bioanalyzer (range average size 445-524 base pairs [bp]). Clustering and DNA sequencing (50-82 million 150-bp paired-end reads) using the NovaSeq6000 DNA sequencer (Illumina) was performed according to manufacturer's protocols. Image analysis, base calling and quality check were performed with the Illumina data analysis pipeline RTA3.4.4 and Bcl2fastq (v2.20).

Prior to alignment, the reads were trimmed for adapter sequences using Trimmomatic (v0.30). Reads were aligned to the *Homo sapiens* reference genome (GRCh37.75) using Tophat (v2.0.14) and read counts were determined using HTSeq (v0.6.1p1). Additionally, transcripts per million (TPM) values were calculated to compare gene expression levels between groups. Differential gene expression was assessed by analyzing read counts with the DESeq2 package (v1.14.1) in the R platform (v3.3.0). Genes with an absolute log₂ fold change >1.0 (*i.e.* a >twofold absolute change) and false discovery rate (FDR)-corrected $P < 0.001$ were considered differentially expressed. Comparison of differentially expressed genes (DEGs) between clones was limited to genes with >1 TPM in the proliferative state or at day 12 of cardiomyogenic differentiation to exclude DEGs with very low overall expression. Gene set enrichment analysis was performed in DAVID (v6.8). The RNA-sequencing data described in this study is available at the NCBI's Gene Expression Omnibus (GEO) under GEO accession number GSE156824.

Generation of human embryonic stem cell (hESC)-derived atrial myocytes (hESC-AMs).

NKX2.5^{EGFP/+}-COUP-TFII^{mCherry/+} hESCs, as described before³³, were maintained as undifferentiated colonies in Essential 8 medium on vitronectin (Thermo Fisher Scientific)-coated culture plastics. Differentiation of these cells to atrial myocytes was performed using the previously described spin embryoid body protocol with retinoic acid treatment^{33,39}. To generate pure populations of hESC-AMs, EGFP and mCherry-double positive cells were purified around day 17 of differentiation using a Sony Biotechnology SH800 flow cytometer after exclusion of dead cells and debris according to side and forward scatter. After sorting, cells were suspended in T10 medium⁵³ and transferred to vitronectin-coated 48-well culture plates (Corning) to establish confluent monolayers. Optical voltage mapping of hESC-AMs was performed 5-11 days after replating.

Cellular electrophysiology. Differentiated hiAMs were dissociated by incubation with a 5 U/mL papain (Worthington Biochemical) and 1 mM L-cysteine (Sigma-Aldrich) solution in PBS for 10 min at 37°C. Next, an equal volume of stop solution was added, consisting of 1 mg/mL soybean trypsin

inhibitor (Sigma-Aldrich) and 40 $\mu\text{g}/\text{mL}$ DNase I (Sigma-Aldrich) in PBS. Cells were pelleted by centrifugation for 5min at $160\times g$ at RT and plated at densities of $3\text{-}6\times 10^4$ cells/ cm^2 on fibronectin-coated 12-mm diameter glass coverslips (Thermo Fisher Scientific), and measured over the three following days.

Single-cell APs were recorded using the amphotericin-perforated patch-clamp technique with Axopatch 200B and MultiClamp 700B amplifiers (Molecular Devices). Signals were low-pass filtered at 5-kHz cut-off frequency and digitized at 40-kHz. Data acquisition and analysis were accomplished with pClamp (v10.7, Molecular Devices) and custom-made software. The bath solution ($36\pm 0.2^\circ\text{C}$) was a modified Tyrode's solution containing (in mM): 140 NaCl, 5.4 KCl, 1.8 CaCl_2 , 1.0 MgCl_2 , 5.5 glucose and 5.0 HEPES-NaOH (pH 7.4). Borosilicate glass patch pipettes (≈ 3 M Ω resistance, Harvard Apparatus) were filled with a solution containing (in mM): 125 K-gluconate, 20 KCl, 5.0 NaCl, 0.44 amphotericin B (Sigma-Aldrich) and 10 HEPES-KOH (pH 7.2). APs were elicited at 1-Hz by 3-ms, $\sim 1.2\times$ threshold current pulses through the patch pipette. Parameters from ten consecutive APs were averaged and potentials were corrected for the calculated liquid junction potential⁵⁴.

Optical voltage mapping. To assess AP properties and propagation in monolayers, hiAMs were seeded in bovine fibronectin-coated 48-well, 24-well or 6-well culture plates at a density of 4×10^5 cells/ cm^2 and differentiated as described. Alternatively, hESC-AMs were seeded at a density of 5.8×10^5 cells/ cm^2 in vitronectin-coated 48-well culture plates. Cell layers of hiAMs or hESC-AMs were incubated with $8\mu\text{M}$ di-4-ANEPPS (Thermo Fisher Scientific) in DMEM/F-12 (11039, Thermo Fisher Scientific) for 10 min in a humidified 95% air-5% CO_2 incubator at 37°C . Following incubation, medium was changed to fresh DMEM/F-12 and cells were placed on a 37°C warming plate for the duration of the experiment.

During optical voltage mapping, excitation light (525 ± 25 nm) was delivered by a halogen arc-lamp through epi-illumination. Emission light passed through a dichroic mirror and a long-pass emission filter (> 590 nm). Signals were acquired using a 100×100 pixels complementary metal oxide semiconductor camera (MiCAM05-Ultima, SciMedia) at a spatial resolution of 165 $\mu\text{m}/\text{pixel}$ (48/24-

well) or 250 $\mu\text{m}/\text{pixel}$ (6-well), and a temporal resolution between 2 and 6 ms per frame depending on the type and duration of experiment. Acquisition times varied between 4 and 12 s for characterization studies, and up to 2 min for arrhythmia studies.

Data was analyzed using BrainVision Analyzer (v16.04.20, BrainVision). Signals were averaged with those of the 8 nearest neighboring pixels to minimize noise artefacts. Conduction velocity (CV), AP duration at 30 and 80% of repolarization (APD_{30} and APD_{80} , respectively) and activation frequency were determined at a minimum of five different vectors/locations equally distributed throughout the culture. Arrhythmia wavelength was calculated by multiplying average CV and APD_{80} in the case of hESC-AMs or CV and reentrant cycle length in the case of hiAMs. Temporal excitation gap was calculated by subtracting APD_{90} during arrhythmic activation from the cycle length. Activation frequency over time was determined by analyzing peak to peak intervals through a custom MATLAB (vR2016a, MathWorks) script on high-pass filtered data at selected locations in the culture.

Electrical stimulation and arrhythmia induction. Electrical point stimulation during optical voltage mapping was performed using an epoxy-coated bipolar platinum electrode, delivering 8-V, 10-ms square pulses. The electrode was connected to a STG 2004 stimulus generator (Multi Channel Systems) driven by MC Stimulus II software (v3.5.0, Multi Channel Systems). Baseline AP properties and propagation were calculated during 1-Hz electrical pacing (*i.e.* 1000-ms cycle length). Restitution was calculated by pacing at a cycle length of 1000 ms (S1) followed by an additional stimulus (S2) at a variable cycle length. Arrhythmia induction was performed by delivering 20 to 40 stimuli at the shortest cycle length at which 1:1 capture was maintained (range 90-180 ms), generally starting with a cycle length equal to the APD_{80} .

Arrhythmia studies and drug interventions. To determine relevant compound dosage, flecainide acetate salt (Sigma-Aldrich) dissolved in DMSO (CryoMACS, Miltenyi Biotec), sotalol hydrochloride (Sigma-Aldrich) dissolved in demineralized water and DMSO (vehicle control), were tested on 2- cm^2

hiAM layers at increasing doses during optical voltage mapping, until loss of excitability. For each compound, three escalating doses were chosen, to include various effect sizes in a clinically relevant range.

Induced reentrant circuits were monitored for 5 min to confirm stability before compounds were infused to study their effect on reentrant circuit characteristics. Flecainide, sotalol or DMSO as control, all at three concentrations, were slowly infused in a 1:1 volume ratio into cultures with reentrant circuits during optical voltage mapping using an infusion pump (Acromed Medical Systems) controlling infusion rate and volume (3 mL at 0.16 mL/s). Cultures were continuously monitored from 2 min prior to drug infusion until 10 min after the start of the drug treatment.

Cryopreservation. hiAMs at day 8 of cardiomyogenic differentiation were dissociated by papain treatment, pelleted by centrifugation and resuspended in cold (4°C) culture medium. Next, an equal volume of ice-cold 80% FBS/20% DMSO was added dropwise to the suspension, after which cryovials containing 10^6 cells/mL were frozen to -80°C at a rate of $-1^{\circ}\text{C}/\text{min}$. Twenty-four h later, the cells were placed in nitrogen vapor for long-term storage. Cells were thawed by swirling vials in a 37°C bath, immediately followed by dropwise addition of cold (4°C) culture medium until a tenfold dilution was reached. Cells were pelleted by centrifugation, resuspended in hiAM differentiation medium and cultured for 6 days in this medium to complete differentiation. Cell viability after dissociation and after thawing as well as replating efficiency of the cells was determined by 0.4% Trypan Blue staining (1:1 ratio, Sigma-Aldrich) and manual counting using a hemocytometer.

Statistical analysis. Statistical analyses were performed using GraphPad Prism (v8.0.1, GraphPad Software). Data are presented as mean \pm standard deviation (SD), unless otherwise indicated. Normally distributed data between independent groups was tested for statistical significance using the unpaired *t*-test (two groups) or using the one-way analysis of variance with Tukey *post-hoc* analysis (three or more groups). Dependent groups were tested using a paired *t*-test (two groups) or using a repeated measure

one-way analysis of variance with Tukey *post-hoc* analysis (three or more groups). The stability of mean CV and APD at various PDs was tested by calculating the Pearson correlation coefficient. Rates of reentrant activity termination were compared between groups using the Chi-square test. A description of the statistical RNA-sequencing data analysis can be found in the supplemental material and methods. All testing was performed two-sided. Statistical significance was expressed as following: * $P < 0.05$, ** $P < 0.01$, *** $P < 0.001$.

DATA AND MATERIALS AVAILABILITY

LV.iMHCK7.SV40-LT-WT particles and hiAM lines can be obtained by academic research groups under a material transfer agreement. All data associated with this study are available in the main text or the supplementary materials. The RNA-sequencing data described in this study is available at the NCBI's Gene Expression Omnibus (GEO) under GEO accession number GSE156824.

REFERENCES

- 1 Robinson, N. B. *et al.* The current state of animal models in research: A review. *Int J Surg* **72**, 9-13, doi:10.1016/j.ijsu.2019.10.015 (2019).
- 2 Ruijtenberg, S. & van den Heuvel, S. Coordinating cell proliferation and differentiation: Antagonism between cell cycle regulators and cell type-specific gene expression. *Cell Cycle* **15**, 196-212, doi:10.1080/15384101.2015.1120925 (2016).
- 3 Thomson, J. A. *et al.* Embryonic stem cell lines derived from human blastocysts. *Science* **282**, 1145-1147, doi:10.1126/science.282.5391.1145 (1998).
- 4 Takahashi, K. *et al.* Induction of pluripotent stem cells from adult human fibroblasts by defined factors. *Cell* **131**, 861-872, doi:10.1016/j.cell.2007.11.019 (2007).
- 5 Yu, J. *et al.* Induced pluripotent stem cell lines derived from human somatic cells. *Science* **318**, 1917-1920, doi:10.1126/science.1151526 (2007).
- 6 Kim, J., Koo, B. K. & Knoblich, J. A. Human organoids: model systems for human biology and medicine. *Nat Rev Mol Cell Biol*, doi:10.1038/s41580-020-0259-3 (2020).
- 7 Liu, J. *et al.* Generation and primary characterization of iAM-1, a versatile new line of conditionally immortalized atrial myocytes with preserved cardiomyogenic differentiation capacity. *Cardiovasc Res* **114**, 1848-1859, doi:10.1093/cvr/cvy134 (2018).
- 8 Liu, J. *et al.* Conditionally immortalized brown preadipocytes can switch between proliferative and differentiated states. *Biochim Biophys Acta Mol Cell Biol Lipids* **1864**, 158511, doi:10.1016/j.bbali.2019.08.007 (2019).
- 9 Deuschle, U., Meyer, W. K. & Thiesen, H. J. Tetracycline-reversible silencing of eukaryotic promoters. *Mol Cell Biol* **15**, 1907-1914, doi:10.1128/mcb.15.4.1907 (1995).
- 10 Szulc, J., Wiznerowicz, M., Sauvain, M. O., Trono, D. & Aebischer, P. A versatile tool for conditional gene expression and knockdown. *Nat Methods* **3**, 109-116, doi:10.1038/nmeth846 (2006).
- 11 Chugh, S. S. *et al.* Worldwide epidemiology of atrial fibrillation: a Global Burden of Disease 2010 Study. *Circulation* **129**, 837-847, doi:10.1161/CIRCULATIONAHA.113.005119 (2014).
- 12 Kim, M. H., Johnston, S. S., Chu, B. C., Dalal, M. R. & Schulman, K. L. Estimation of total incremental health care costs in patients with atrial fibrillation in the United States. *Circ Cardiovasc Qual Outcomes* **4**, 313-320, doi:10.1161/CIRCOUTCOMES.110.958165 (2011).
- 13 Nattel, S., Heijman, J., Zhou, L. & Dobrev, D. Molecular Basis of Atrial Fibrillation Pathophysiology and Therapy: A Translational Perspective. *Circ Res* **127**, 51-72, doi:10.1161/CIRCRESAHA.120.316363 (2020).
- 14 Heijman, J., Guichard, J. B., Dobrev, D. & Nattel, S. Translational Challenges in Atrial Fibrillation. *Circ Res* **122**, 752-773, doi:10.1161/CIRCRESAHA.117.311081 (2018).
- 15 Kirchhof, P. The future of atrial fibrillation management: integrated care and stratified therapy. *Lancet* **390**, 1873-1887, doi:10.1016/S0140-6736(17)31072-3 (2017).
- 16 van Gorp, P. R. R., Trines, S. A., Pijnappels, D. A. & de Vries, A. A. F. Multicellular In vitro Models of Cardiac Arrhythmias: Focus on Atrial Fibrillation. *Front Cardiovasc Med* **7**, 43, doi:10.3389/fcvm.2020.00043 (2020).
- 17 Salva, M. Z. *et al.* Design of tissue-specific regulatory cassettes for high-level rAAV-mediated expression in skeletal and cardiac muscle. *Mol Ther* **15**, 320-329, doi:10.1038/sj.mt.6300027 (2007).
- 18 Huttenbach, Y., Ostrowski, M. L., Thaller, D. & Kim, H. S. Cell proliferation in the growing human heart: MIB-1 immunostaining in preterm and term infants at autopsy. *Cardiovasc Pathol* **10**, 119-123, doi:10.1016/s1054-8807(01)00065-5 (2001).
- 19 Baker, M. Reproducibility: Respect your cells! *Nature* **537**, 433-435, doi:10.1038/537433a (2016).
- 20 Narayan, S. M., Shivkumar, K., Krummen, D. E., Miller, J. M. & Rappel, W. J. Panoramic electrophysiological mapping but not electrogram morphology identifies stable sources for human atrial fibrillation: stable atrial fibrillation rotors and focal sources relate poorly to fractionated electrograms. *Circ Arrhythm Electrophysiol* **6**, 58-67, doi:10.1161/CIRCEP.111.977264 (2013).

- 21 Balouch, M. *et al.* Impact of rotor temperospatial stability on acute and one-year atrial fibrillation ablation outcomes. *Clin Cardiol* **40**, 383-389, doi:10.1002/clc.22674 (2017).
- 22 Laksman, Z. *et al.* Modeling Atrial Fibrillation using Human Embryonic Stem Cell-Derived Atrial Tissue. *Sci Rep* **7**, 5268, doi:10.1038/s41598-017-05652-y (2017).
- 23 Sanders, P. *et al.* Spectral analysis identifies sites of high-frequency activity maintaining atrial fibrillation in humans. *Circulation* **112**, 789-797, doi:10.1161/CIRCULATIONAHA.104.517011 (2005).
- 24 Schuessler, R. B. *et al.* Spatial and temporal stability of the dominant frequency of activation in human atrial fibrillation. *J Electrocardiol* **39**, S7-12, doi:10.1016/j.jelectrocard.2006.04.009 (2006).
- 25 Yoshida, K. *et al.* Left atrial pressure and dominant frequency of atrial fibrillation in humans. *Heart Rhythm* **8**, 181-187, doi:10.1016/j.hrthm.2010.10.030 (2011).
- 26 January, C. T. *et al.* 2014 AHA/ACC/HRS guideline for the management of patients with atrial fibrillation: a report of the American College of Cardiology/American Heart Association Task Force on Practice Guidelines and the Heart Rhythm Society. *J Am Coll Cardiol* **64**, e1-76, doi:10.1016/j.jacc.2014.03.022 (2014).
- 27 Kirchhof, P. *et al.* 2016 ESC Guidelines for the management of atrial fibrillation developed in collaboration with EACTS. *Eur Heart J* **37**, 2893-2962, doi:10.1093/eurheartj/ehw210 (2016).
- 28 Hindricks, G. *et al.* 2020 ESC Guidelines for the diagnosis and management of atrial fibrillation developed in collaboration with the European Association of Cardio-Thoracic Surgery (EACTS). *Eur Heart J*, doi:10.1093/eurheartj/ehaa612 (2020).
- 29 Sanguinetti, M. C. & Jurkiewicz, N. K. Two components of cardiac delayed rectifier K⁺ current. Differential sensitivity to block by class III antiarrhythmic agents. *J Gen Physiol* **96**, 195-215, doi:10.1085/jgp.96.1.195 (1990).
- 30 Melgari, D., Zhang, Y., El Harchi, A., Dempsey, C. E. & Hancox, J. C. Molecular basis of hERG potassium channel blockade by the class Ic antiarrhythmic flecainide. *J Mol Cell Cardiol* **86**, 42-53, doi:10.1016/j.yjmcc.2015.06.021 (2015).
- 31 Davidson, M. M. *et al.* Novel cell lines derived from adult human ventricular cardiomyocytes. *J Mol Cell Cardiol* **39**, 133-147, doi:10.1016/j.yjmcc.2005.03.003 (2005).
- 32 Goldman, B. I., Amin, K. M., Kubo, H., Singhal, A. & Wurzel, J. Human myocardial cell lines generated with SV40 temperature-sensitive mutant tsA58. *In Vitro Cell Dev Biol Anim* **42**, 324-331, doi:10.1290/0605032.1 (2006).
- 33 Schwach, V. *et al.* A COUP-TFII Human Embryonic Stem Cell Reporter Line to Identify and Select Atrial Cardiomyocytes. *Stem Cell Reports* **9**, 1765-1779, doi:10.1016/j.stemcr.2017.10.024 (2017).
- 34 Ban, K., Bae, S. & Yoon, Y. S. Current Strategies and Challenges for Purification of Cardiomyocytes Derived from Human Pluripotent Stem Cells. *Theranostics* **7**, 2067-2077, doi:10.7150/thno.19427 (2017).
- 35 Lee, J. H., Protze, S. I., Laksman, Z., Backx, P. H. & Keller, G. M. Human Pluripotent Stem Cell-Derived Atrial and Ventricular Cardiomyocytes Develop from Distinct Mesoderm Populations. *Cell Stem Cell* **21**, 179-194 e174, doi:10.1016/j.stem.2017.07.003 (2017).
- 36 Argenziano, M. *et al.* Electrophysiologic Characterization of Calcium Handling in Human Induced Pluripotent Stem Cell-Derived Atrial Cardiomyocytes. *Stem Cell Reports* **10**, 1867-1878, doi:10.1016/j.stemcr.2018.04.005 (2018).
- 37 Branco, M. A. *et al.* Transcriptomic analysis of 3D Cardiac Differentiation of Human Induced Pluripotent Stem Cells Reveals Faster Cardiomyocyte Maturation Compared to 2D Culture. *Sci Rep* **9**, 9229, doi:10.1038/s41598-019-45047-9 (2019).
- 38 Buikema, J. W. *et al.* Wnt Activation and Reduced Cell-Cell Contact Synergistically Induce Massive Expansion of Functional Human iPSC-Derived Cardiomyocytes. *Cell Stem Cell* **27**, 50-63 e55, doi:10.1016/j.stem.2020.06.001 (2020).
- 39 Devalla, H. D. *et al.* Atrial-like cardiomyocytes from human pluripotent stem cells are a robust preclinical model for assessing atrial-selective pharmacology. *EMBO Mol Med* **7**, 394-410, doi:10.15252/emmm.201404757 (2015).

- 40 Voigt, N. *et al.* Enhanced sarcoplasmic reticulum Ca²⁺ leak and increased Na⁺-Ca²⁺ exchanger function underlie delayed afterdepolarizations in patients with chronic atrial fibrillation. *Circulation* **125**, 2059-2070, doi:10.1161/CIRCULATIONAHA.111.067306 (2012).
- 41 Voigt, N. *et al.* Cellular and molecular mechanisms of atrial arrhythmogenesis in patients with paroxysmal atrial fibrillation. *Circulation* **129**, 145-156, doi:10.1161/CIRCULATIONAHA.113.006641 (2014).
- 42 Heijman, J. *et al.* Atrial Myocyte NLRP3/CaMKII Nexus Forms a Substrate for Post-Operative Atrial Fibrillation. *Circ Res*, doi:10.1161/CIRCRESAHA.120.316710 (2020).
- 43 Nakanishi, H. *et al.* Geometrical Patterning and Constituent Cell Heterogeneity Facilitate Electrical Conduction Disturbances in a Human Induced Pluripotent Stem Cell-Based Platform: An In vitro Disease Model of Atrial Arrhythmias. *Front Physiol* **10**, 818, doi:10.3389/fphys.2019.00818 (2019).
- 44 Goldfracht, I. *et al.* Generating ring-shaped engineered heart tissues from ventricular and atrial human pluripotent stem cell-derived cardiomyocytes. *Nat Commun* **11**, 75, doi:10.1038/s41467-019-13868-x (2020).
- 45 Harrild, D. & Henriquez, C. A computer model of normal conduction in the human atria. *Circ Res* **87**, E25-36, doi:10.1161/01.res.87.7.e25 (2000).
- 46 Valderrabano, M. Influence of anisotropic conduction properties in the propagation of the cardiac action potential. *Prog Biophys Mol Biol* **94**, 144-168, doi:10.1016/j.pbiomolbio.2007.03.014 (2007).
- 47 Salvage, S. C. *et al.* Multiple targets for flecainide action: implications for cardiac arrhythmogenesis. *Br J Pharmacol* **175**, 1260-1278, doi:10.1111/bph.13807 (2018).
- 48 Lemme, M. *et al.* Atrial-like Engineered Heart Tissue: An In Vitro Model of the Human Atrium. *Stem Cell Reports* **11**, 1378-1390, doi:10.1016/j.stemcr.2018.10.008 (2018).
- 49 Zhao, Y. *et al.* A Platform for Generation of Chamber-Specific Cardiac Tissues and Disease Modeling. *Cell* **176**, 913-927 e918, doi:10.1016/j.cell.2018.11.042 (2019).
- 50 Lee, A. *et al.* 3D bioprinting of collagen to rebuild components of the human heart. *Science* **365**, 482-487, doi:10.1126/science.aav9051 (2019).
- 51 Yu, H. & Wang, Z. Cardiomyocyte-Derived Exosomes: Biological Functions and Potential Therapeutic Implications. *Front Physiol* **10**, 1049, doi:10.3389/fphys.2019.01049 (2019).
- 52 Goette, A. *et al.* EHRA/HRS/APHS/SOLAECE expert consensus on atrial cardiomyopathies: Definition, characterization, and clinical implication. *Heart Rhythm* **14**, e3-e40, doi:10.1016/j.hrthm.2016.05.028 (2017).
- 53 Birket, M. J. *et al.* Contractile Defect Caused by Mutation in MYBPC3 Revealed under Conditions Optimized for Human PSC-Cardiomyocyte Function. *Cell Rep* **13**, 733-745, doi:10.1016/j.celrep.2015.09.025 (2015).
- 54 Barry, P. H. & Lynch, J. W. Liquid junction potentials and small cell effects in patch-clamp analysis. *J Membr Biol* **121**, 101-117, doi:10.1007/BF01870526 (1991).

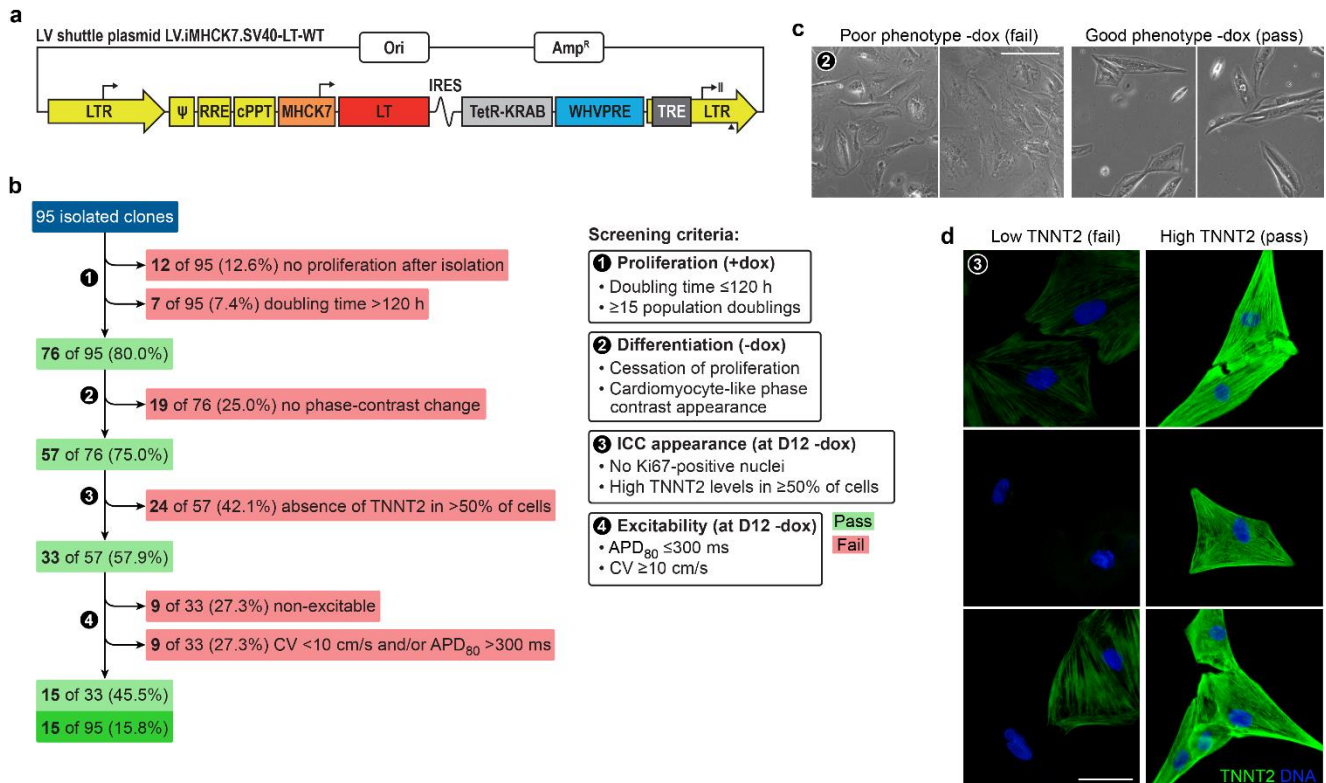
Acknowledgments: The authors thank Jia Liu (LUMC, Leiden, the Netherlands) for constructing plasmid pLV.iMHCK7.SV40-LT-WT and producing LV.iMHCK7.SV40-LT-WT particles, Tessa van Herwaarden (LUMC, Leiden, the Netherlands) for collecting human fetal atrial tissue, Bini Klein (LUMC, Leiden, the Netherlands) for donating the SV40 LT-encoding plasmid pAT153.SV40ori, Stephen Hauschka (University of Washington, Seattle, WA) for providing construct +aMHCKChCAT encoding the MHCK7 promoter, Didier Trono (Swiss Federal Institute of Technology Lausanne, Lausanne, Switzerland) for making available the LV shuttle plasmid pLVET-tTR-KRAB and Ursula Ravens (University of Freiburg, Freiburg, Germany) for useful discussions.

Funding: This publication received financial support from the research programme ‘More Knowledge with Fewer Animals’ (MKMD, project 114022503, to A.A.F.d.V.), which is (partly) financed by the Netherlands Organisation for Health Research and Development (ZonMw) and by the Dutch Society for the Replacement of Animal Testing (dsRAT). Additional support was provided by the Leiden Regenerative Medicine Platform Holding (LRMPH project 8212/41235 to A.A.F.d.V.).

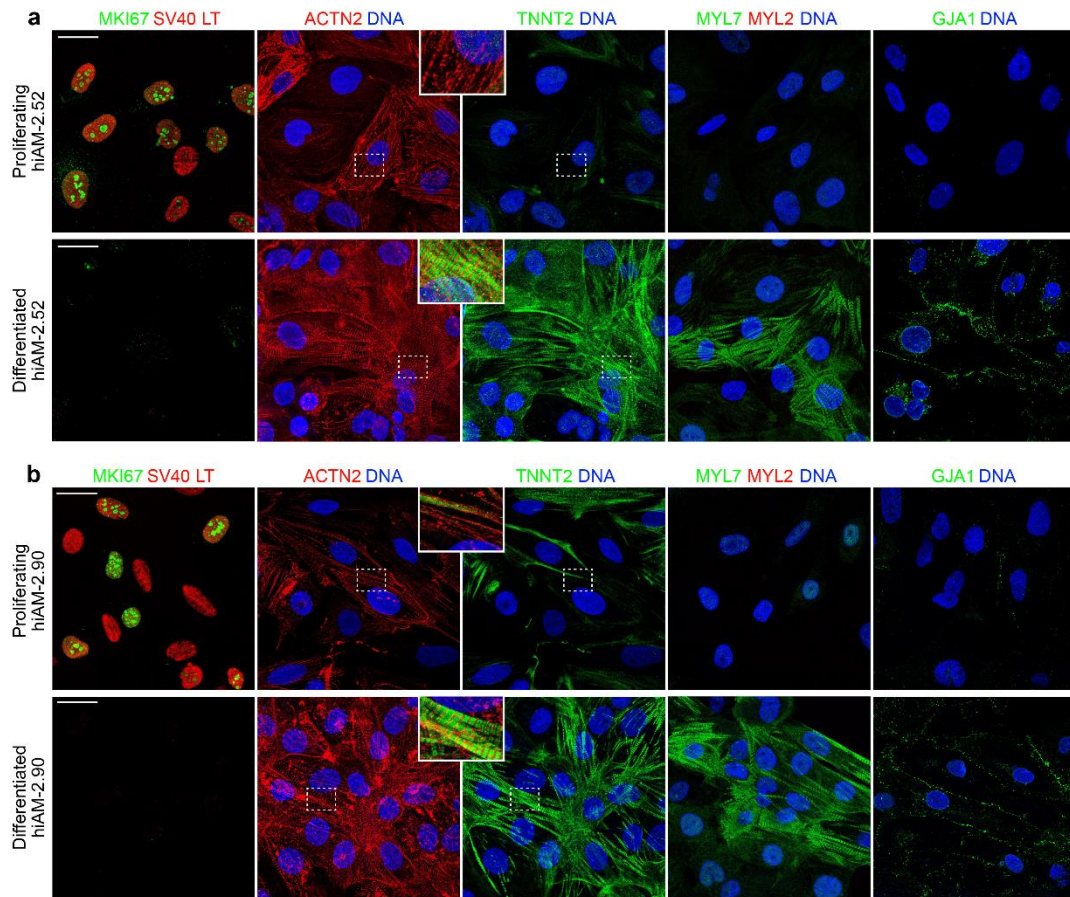
Author contributions: N.H., D.A.P. and A.A.F.d.V. conceived the study, interpreted results and wrote the manuscript. N.H. with assistance of S.O.D, J.Z. and L.J.S.L generated and characterized the hiAM lines. M.W.V., A.O.V. and M.R.R. performed and analyzed patch-clamping experiments. V.S., C.C.F. and R.P. generated hESC-AM layers and assisted with the associated analyses. M.J.T.H.G. provided human fetal atrial material. D.D. assisted in the design and interpretation of the arrhythmia studies. T.J.v.B., R.J.M.K. and M.J.S. provided clinical input on the study. All authors refined the manuscript.

Competing interests: M.J.S., D.A.P. and A.A.F.d.V. are inventors on a patent application (US16/480,280, “Conditionally immortalized cells and methods for their preparation”) related to this work. R.P. is a cofounder of Pluriomics (Ncardia) and River Biomedics. Revenues resulting from hiAM culture media services provided by the LUMC will be deployed for non-commercial academic research purposes. D.D. is a member of the scientific advisory boards of OMEICOS Therapeutics and Acesion Pharma. All other authors declare that they have no competing interests.

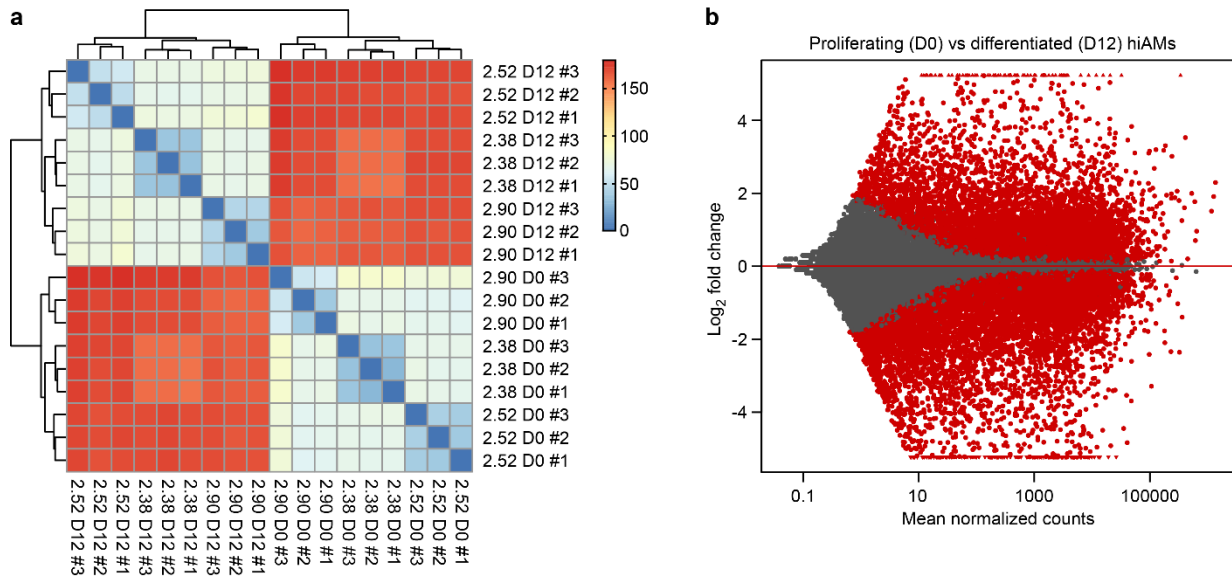
SUPPLEMENTARY INFORMATION



Supplementary Fig. 1: Extended data on the generation and selection of hiAM monoclones. (a) LV shuttle plasmid LV.iMHCK7.SV40-LT-WT. Ori, bacterial origin of replication. Amp^R, *Escherichia coli* β-lactamase gene. LTR, human immunodeficiency virus type 1 (HIV1) long terminal repeat. ψ, HIV1 packaging signal. RRE, HIV1 Rev-responsive element. cPPT, HIV1 central polypurine tract and termination site. MHCK7, chimeric striated muscle-specific promoter. LT, coding sequence of wildtype oncogenic SV40 LT antigen. IRES, encephalomyocarditis virus internal ribosome entry site. TetR-KRAB, coding sequence of hybrid tetracycline-controlled transcriptional repressor. WHVPRE, woodchuck hepatitis virus posttranscriptional regulatory element. TRE, tetracycline-responsive promoter element consisting of 7 repeats of a 19-nucleotide tetracycline operator (tetO) sequence. (b) Extended flowchart of hiAM clone selection based on four main criteria with corresponding drop-off rates. ICC, Immunocytochemistry. TNNT2, cardiac troponin T. (c) Example of two hiAM monoclonal displaying no cardiomyocyte-like change in phase contrast and of two monoclonal showing a cardiomyocyte-like alteration in phase contrast after 12 days of culture in the absence of dox (criterion 2, differentiation). Scale bar, 100 μm. (d) Example of three hiAM monoclonal that do and of three hiAM clones that do not pass the third criterion (*i.e.* immunocytochemical appearance) due to low and high TNNT2 expression, respectively, as assessed by ICC. Scale bar, 50 μm.

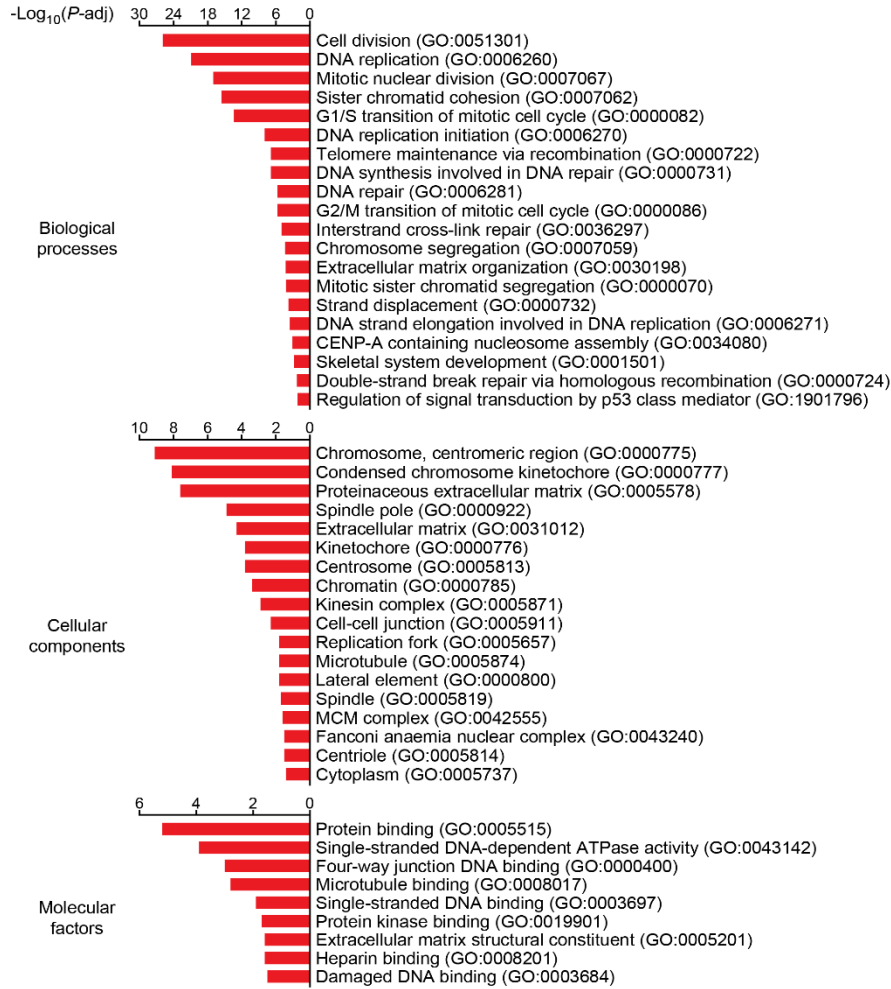


Supplementary Fig. 2: Immunocytochemical characterization of the structure of hiAM clones 2.52 and 2.90 during proliferating and after 12 days of differentiation. Proliferating and differentiated (a) hiAM-2.52 and (b) hiAM-2.90 were immunostained for Ki-67 (MKI67), SV40 LT, α -actinin (ACTN2), cardiac muscle troponin T (TNNT2), the atrial and ventricular isoform of myosin regulatory light chain 2 (MYL7 and MYL2, respectively) and connexin 43 (GJA1). Scale bar, 25 μ m.

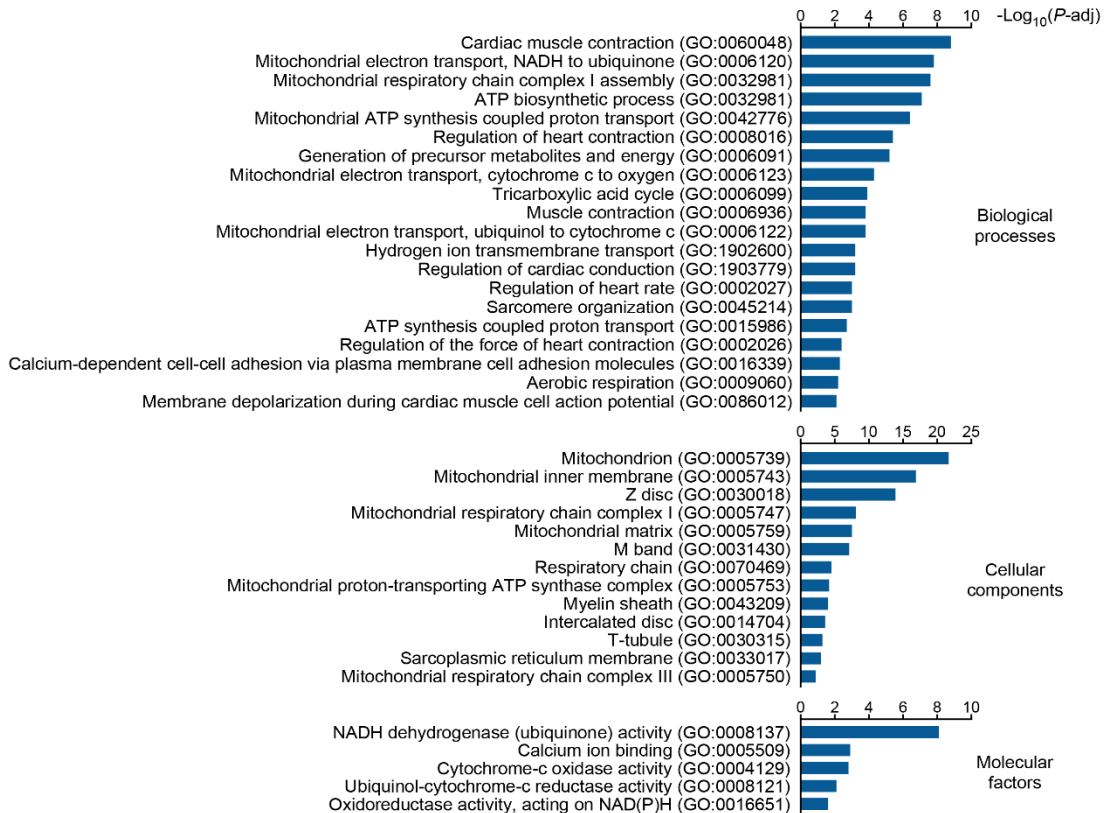


Supplementary Fig. 3: RNA-sequencing data of proliferating (D0) and differentiated (D12) hiAMs. (a) Heatmap for all samples, based on relative distances of the samples. The difference in gene expression profile between the samples increases moving from blue to red. (b) MA plot depicting successful normalization of gene expression ($\alpha = 0.05$). D0, Zero days without dox. D12, Twelve days without dox.

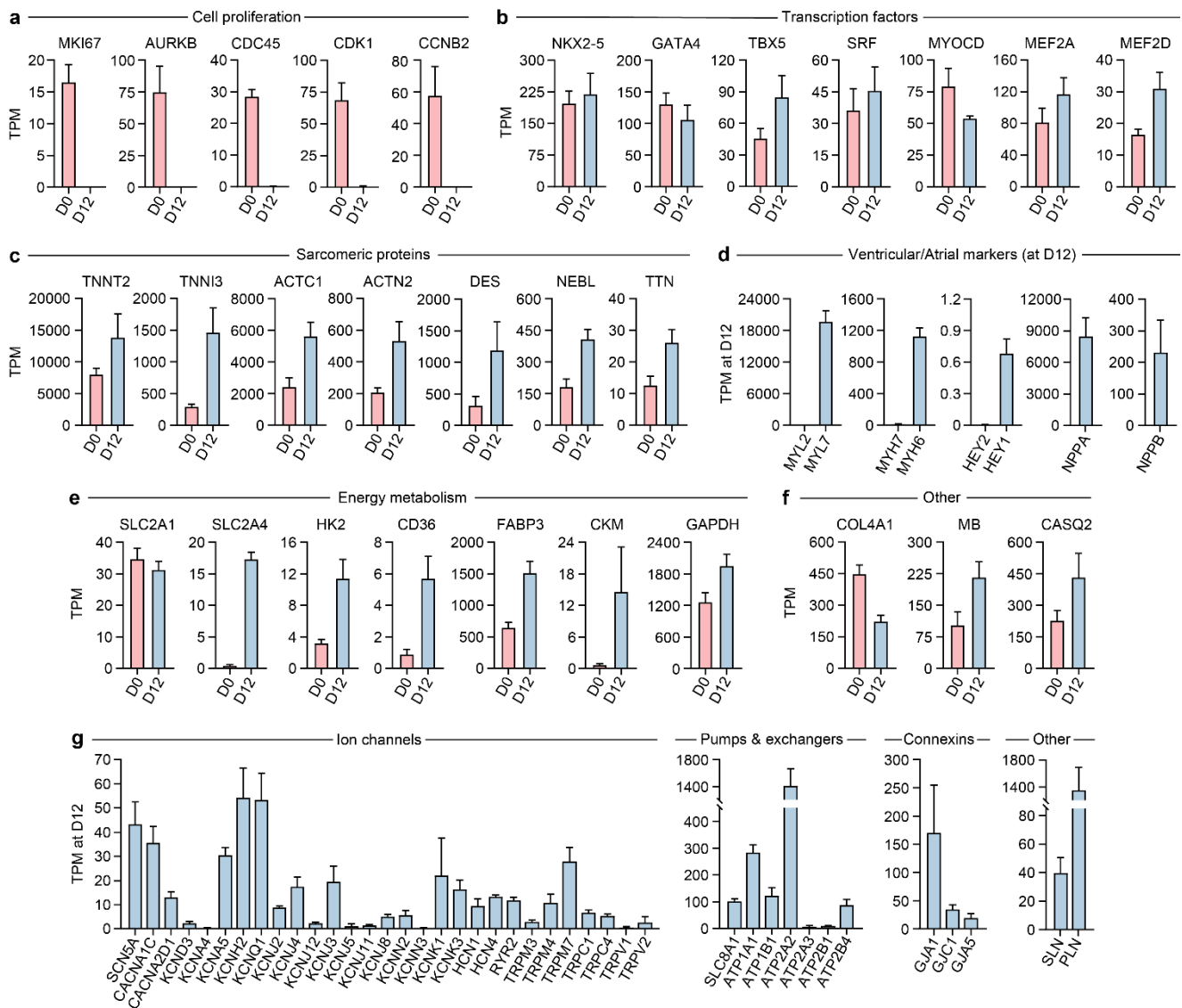
Enriched in proliferating hiAMs



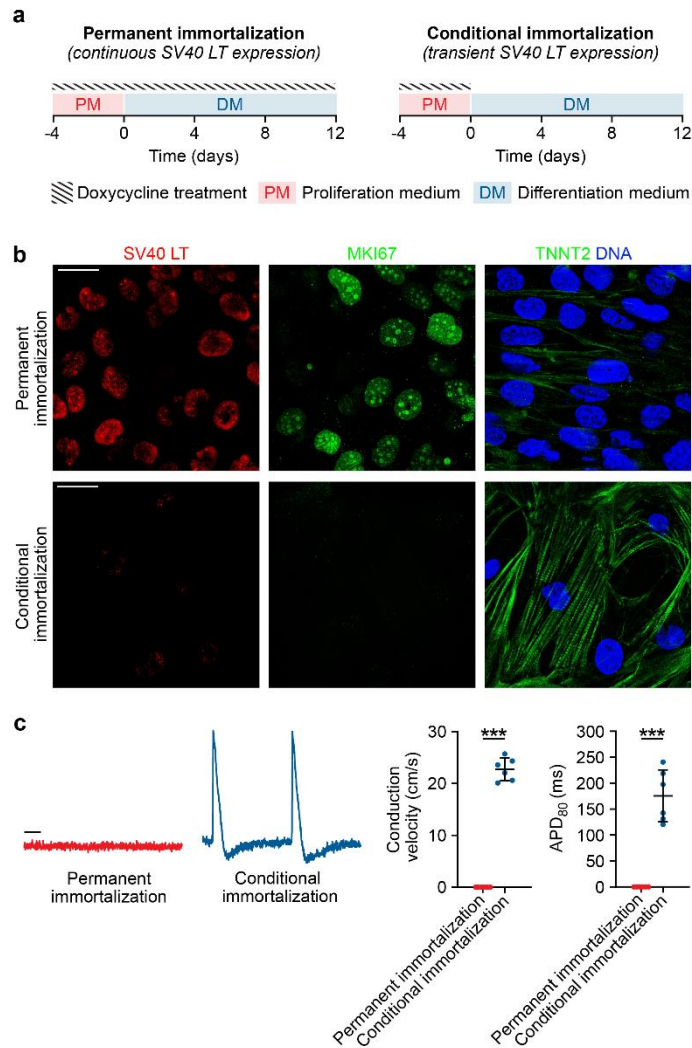
Enriched in differentiated hiAMs



Supplementary Fig. 4: Extended data on gene set enrichment analysis. Enriched GO terms (P -adjusted < 0.05) in proliferating hiAMs (left, red) and in differentiated hiAMs (blue, right).

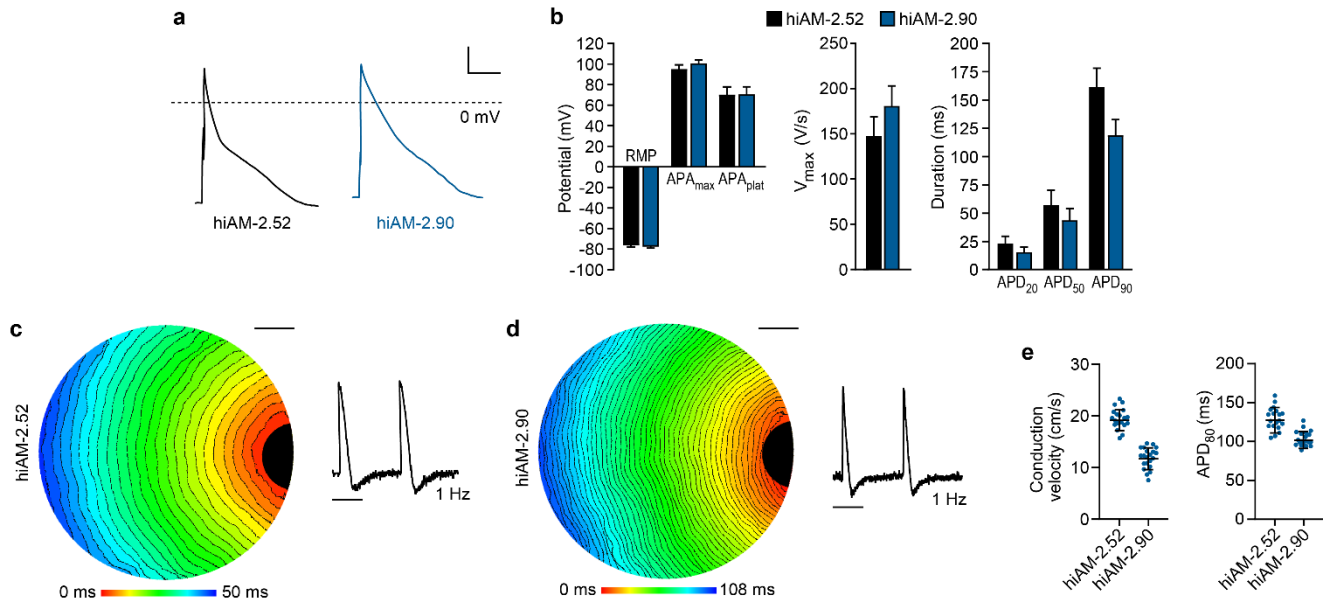


Supplementary Fig. 5: Gene expression analysis by RNA-sequencing of hiAMs during proliferation (D0) and after differentiation (D12). TPM are shown of genes (a) involved in cell proliferation, (b) encoding cardiac transcription factors, (c) coding for cardiac sarcomeric proteins, (d) preferentially expressed in atrial or ventricular cardiomyocytes, (e) involved in energy metabolism, and (f) encoding some other relevant genes. (g) TPM in differentiated hiAMs of genes involved in excitability, calcium handling and electrical coupling. Bars represent mean gene expression levels in hiAM clones 2.38, 2.52 and 2.90 ($n = 3$ replicates per clone per time point). Error bars indicate SD. D0, Zero days without dox. D12, Twelve days without dox.

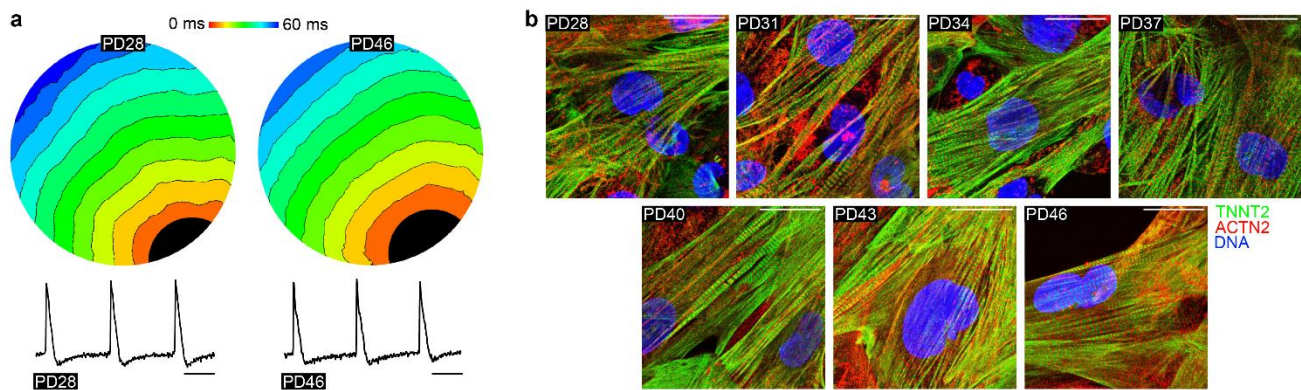


Supplementary Fig. 6: Permanent cell immortalization versus conditional cell immortalization.

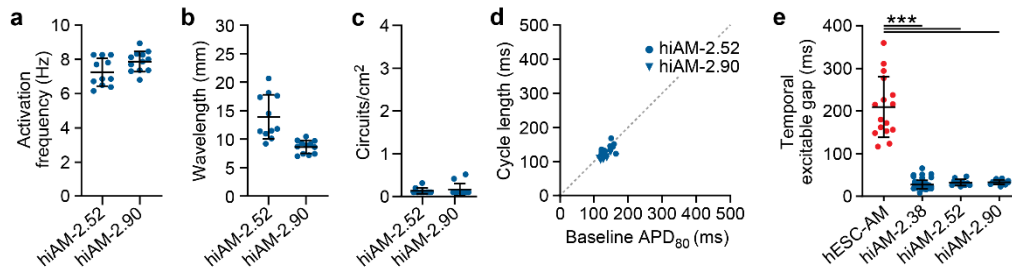
(a) Schematic overview of permanent immortalization (achieved through the continuous presence of dox) versus conditional immortalization. In both cases, the proliferation medium was replaced by differentiation medium 12 days before analysis. (b) Immunofluorographs of hiAMs stained for Ki-67 (MKI67), SV40 LT and cardiac muscle troponin T (TNNT2) after 12 days of culture in differentiation medium. Scale bar, 25 μ m. (c) Optical voltage mapping traces (left), CV and APD₈₀ (right) after 12 days of culture in differentiation medium. Permanent SV40 LT expression precludes cardiomyogenic differentiation of hiAMs as evinced by the absence of excitable cells after 12 days of culture in differentiation medium. Scale bar, 200 ms. $n = 6$ from 2 independent differentiations. *** $P < 0.001$, unpaired t -test.



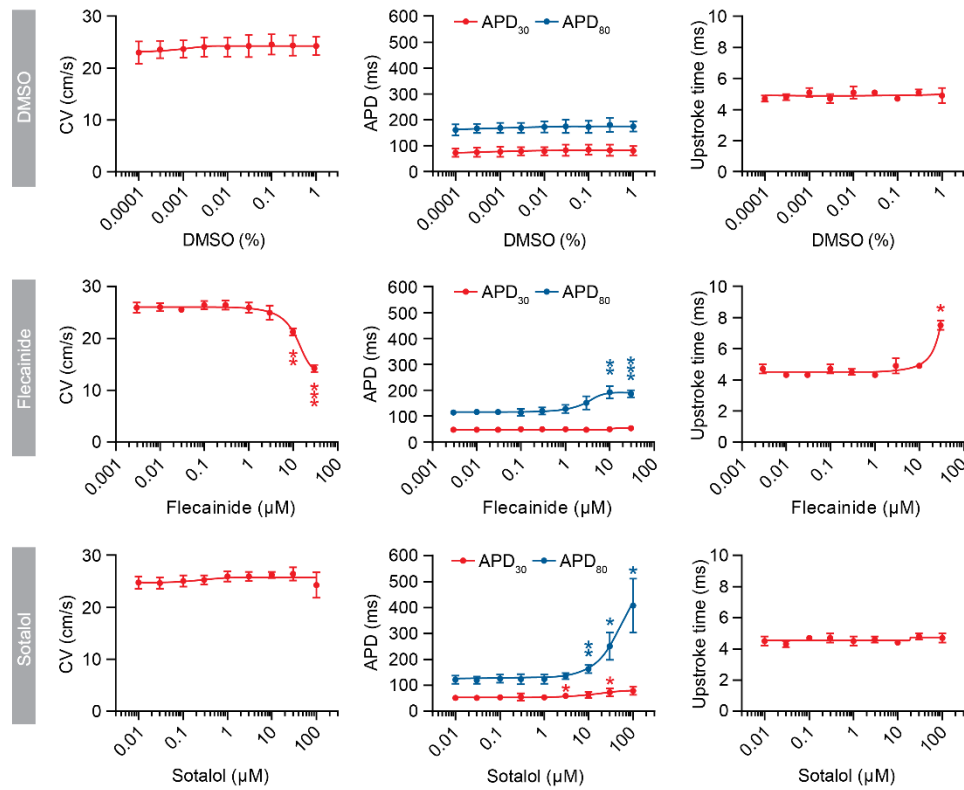
Supplementary Fig. 7: Electrophysiological characterization of differentiated hiAM clones 2.52 and 2.90. (a) Representative AP traces and (b) mean AP parameters of single differentiated hiAM-2.52 ($n = 13$ cells from 3 independent preparations) and single differentiated hiAM-2.90 ($n = 14$ cells from 3 independent differentiations) during 1-Hz electrical stimulation. Scale bars in (a) $x = 50$ ms, $y = 20$ mV. Dotted line in (a) indicates the zero mV level. Error bars indicate standard error of the mean. (c, d) Representative activation maps and optical voltage traces of differentiated (c) hiAM-2.52 and (d) hiAM-2.90 layers (24-well format). Isochrones, 2 ms. Scale bar of maps, 2 mm. Scale bar of traces, 500 ms. (e) Mean CV and APD₈₀ in confluent layers of differentiated hiAM-2.52 ($n = 19$ from 4 independent experiments) and hiAM-2.90 ($n = 21$ from 3 independent experiments). Error bars indicate SD.



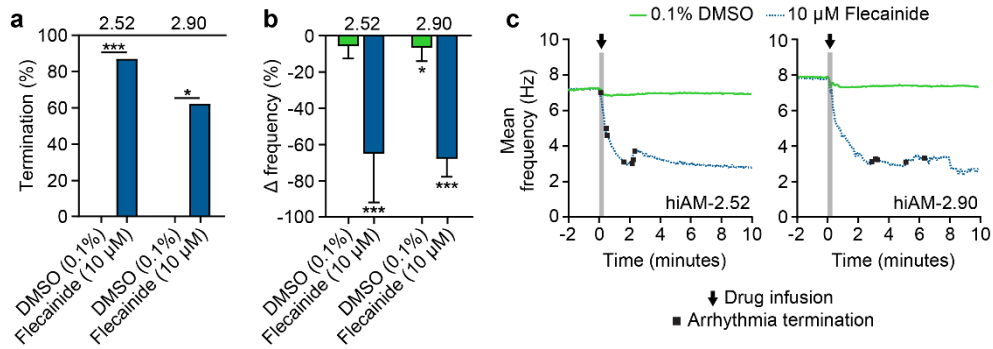
Supplementary Fig. 8: Differentiation capacity of hiAMs at different PDs. (a) Representative activation map and optical voltage traces of differentiated hiAM-2.38 layer at PD 28 and at PD 46 (24-well format). Isochrones, 6 ms. Scale bar, 500 ms. (b) Immunostaining patterns of α -actinin (ACTN2) and cardiac troponin T (TNNT2) of differentiated hiAMs at different PDs. Scale bar, 25 μ m.



Supplementary Fig. 9: Arrhythmia characteristics of differentiated hiAM clone 2.52 and 2.90 cultures. (a) Mean activation frequency, (b) wavelength and (c) arrhythmia complexity (*i.e.* the number of reentrant circuits per cm^2) of hiAM-2.52 and hiAM-2.90 cultures following induction of reentrant circuits. (d) Correlation between baseline APD_{80} and cycle length of induced reentrant circuits in hiAM-2.52 and hiAM-2.90 cultures. (e) Temporal excitable gap in arrhythmic hESC-AM and hiAM clone 2.38, 2.52 and 2.90 cultures. hESC-AM: $n = 7$ independent cultures, hiAM-2.38: $n = 56$ independent cultures. $***P < 0.001$, one-way analysis of variance with Tukey *post-hoc* analysis. (a-e) hiAM-2.52: $n = 11$ independent cultures, hiAM-2.90: $n = 12$ independent cultures.



Supplementary Fig. 10: Dose-dependent effects of flecainide and sotalol on differentiated hiAM cultures. Effects of DMSO (solvent/vehicle control), flecainide and sotalol at increasing concentrations on CV, APD_{30/80} and upstroke time in differentiated 2-cm² hiAM-2.38 cultures as measured by optical voltage mapping. Concentrations were increased until cultures were no longer excitable. $n = 5$ cultures for each group. Error bars indicate SD. * $P < 0.05$, ** $P < 0.01$, *** $P < 0.001$, repeated measures analysis of variance with Tukey *post-hoc* analysis with the lowest concentrations serving as baseline.



Supplementary Fig. 11: Effects of flecainide on arrhythmic hiAM clone 2.52 and 2.90 cultures. (a) Rate of reentrant circuit termination and **(b)** change (Δ) in activation frequency in arrhythmic 10-cm² cultures of differentiated hiAM-2.52 and hiAM-2.90 following 10 min after infusion of 0.1% DMSO or 10 μ M flecainide compared to baseline. **(c)** Continuous monitoring of mean activation frequency in arrhythmic hiAM-clone 2.52 and 2.90 cultures prior to and after infusion of 0.1% DMSO or 10 μ M flecainide. **(a-c)** $n = 8$ for each compound and hiAM clone. Error bars indicate SD. * $P < 0.05$, *** $P < 0.001$. **(a)** Chi-square test. **(b)** Unpaired t -test.

Supplementary Table 1 - AP parameters of hfAMs and hiAMs

Parameter	hfAM (n = 6)	hiAM-2.38 (n = 21)	hiAM-2.52 (n = 13)	hiAM-2.90 (n = 14)
RMP (mV)	-74.5 (1.0)	-81.9 (1.1)***	-76.5 (1.2)	-77.9 (0.9)*
APA _{max} (mV)	85.2 (6.0)	105.5 (2.9)***	95.4 (3.7)	101.0 (2.6)**
APA _{plat} (mV)	47.0 (4.0)	62.6 (5.5)	70.5 (7.2)*	71.2 (6.5)*
V _{max} (V/s)	130.2 (27.9)	171.9 (26.1)	147.9 (21.0)	181.2 (21.6)
APD ₂₀ (ms)	5.6 (2.2)	11.8 (2.6)	23.7 (5.8)*	16.1 (3.7)
APD ₅₀ (ms)	37.1 (15.1)	36.4 (7.7)	57.6 (12.6)	44.1 (10.1)
APD ₉₀ (ms)	151.6 (26.7)	151.6 (17.0)	161.9 (16.5)	119.3 (13.3)

Data presented as mean (SEM). * $P < 0.05$, ** $P < 0.01$, *** $P < 0.001$, unpaired t -test compared with hfAM.

Supplementary Table 2 - Antibodies

Antigen	Host	Dilution	Supplier	Catalogue number	
SV40 LT	Mouse	1:400 (ICC) 1:5000 (WB)	Santa Cruz Biotechnology	sc-147	
MKI67	Rabbit	1:400 (ICC)	Abcam	ab15580	
ACTN2	Mouse	1:400 (ICC)	Sigma-Aldrich	A7811	
TNNT2	Rabbit	1:400 (ICC)	Abcam	ab45932	
MYL7	Rabbit	1:400 (ICC)	Abcam	ab127001	
MYL2	Mouse	1:50 (ICC)	Enzo	ALX-BC-1150-S-L001	
GJA1	Rabbit	1:400 (ICC)	Sigma-Aldrich	C6219	
NKX-2.5	Mouse	1:400 (ICC)	Santa Cruz Biotechnology	sc-376565	
GAPDH	Mouse	1:10.000 (WB)	Merck	MAB374	
Antigen	Host	Dilution	Supplier	Catalogue number	Conjugate
Mouse IgG (H+L)	Goat	1:10.000 (WB)	Abcam	ab97040	HRP
Mouse IgG (H+L)	Donkey	1:400 (ICC)	Thermo Fisher Scientific	A10037	Alexa Fluor 568
Rabbit IgG (H+L)	Donkey	1:400 (ICC)	Thermo Fisher Scientific	A21206	Alexa Fluor 488

ICC, immunocytochemistry. WB, western blot. HRP, horseradish peroxidase.

Supplementary Video 1: Contractions of hfAMs and hiAMs. Spontaneous contractions in hfAMs and hiAM-2.38 cultures. Scale bar, 1 mm.

Supplementary Video 2: Optical voltage mapping of hESC-AM and hiAM layers. Optical voltage mapping recordings during 1-Hz electrical stimulation (white dots represent pacing electrode and electrical stimulation). Playback at 1/6 of real time speed. Scale bar, 2 mm.

Supplementary Video 3: Induction of reentrant activity in hESC-AM and hiAM layers. Induction of reentrant activity through high frequency stimulation in hESC-AM and hiAM-2.38 layers (white dots represent pacing electrode and electrical stimulation). Playback at 1/3 of real time speed. Scale bar, 5 mm.

Supplementary Video 4: hiAM arrhythmic activity with varying degrees of complexity. Three examples of atrial arrhythmias of different complexities as determined by the number of reentrant circuits present in the hiAM-2.38 layers following induction. Playback at 1/3 of real time speed. Scale bar, 1 cm.

Supplementary Video 5: Effects of antiarrhythmic drugs on reentrant activity in hiAM layers. Effect of 0.1% DMSO, 30 μ M sotalol and 10 μ M flecainide on reentrant activity in hiAM layers after infusion. DMSO infusion has no effect on arrhythmic activity, whereas 30 μ M sotalol reduces the activation frequency by 34% after 10 minutes. Flecainide (10 μ M) infusion results in termination of arrhythmic activity, after which 1-Hz electrical stimulation results in normal conduction. Playback at 1/3 of real time speed. Scale bar, 5 mm.